Special Report 85-25

December 1985

**US Army Corps
of Engineers**

Cold Regions Research &
Engineering Laboratory

Blasting and blast effects in cold regions

Part I: Air blast

Malcolm Mellor

AD-A166 315

DTIC FILE COPY

DTIC
ELECTE
APR 7 1986
B

86 4 7 065

REPORT DOCUMENTATION PAGE		READ INSTRUCTIONS BEFORE COMPLETING FORM
1. REPORT NUMBER Special Report 85-25	2. GOVT ACCESSION NO.	3. RECIPIENT'S CATALOG NUMBER
4. TITLE *(and Subtitle)* BLASTING AND BLAST EFFECTS IN COLD REGIONS Part I: Air blast		5. TYPE OF REPORT & PERIOD COVERED
		6. PERFORMING ORG. REPORT NUMBER
7. AUTHOR(s) Malcolm Mellor		8. CONTRACT OR GRANT NUMBER(s)
9. PERFORMING ORGANIZATION NAME AND ADDRESS U.S. Army Cold Regions Research and Engineering Laboratory Hanover, New Hampshire 03755-1290		10. PROGRAM ELEMENT, PROJECT, TASK AREA & WORK UNIT NUMBERS 6.27.40A DA Project 4A762730AT42 Task Area Cs, Work Unit 029
11. CONTROLLING OFFICE NAME AND ADDRESS		12. REPORT DATE December 1985
		13. NUMBER OF PAGES 72
14. MONITORING AGENCY NAME & ADDRESS*(if different from Controlling Office)* Office of the Chief of Engineers Washington, D.C. 20314-1000		15. SECURITY CLASS. *(of this report)* Unclassified
		15a. DECLASSIFICATION DOWNGRADING SCHEDULE

16. DISTRIBUTION STATEMENT *(of this Report)*

Approved for public release; distribution is unlimited.

17. DISTRIBUTION STATEMENT *(of the abstract entered in Block 20, if different from Report)*

18. SUPPLEMENTARY NOTES

19. KEY WORDS *(Continue on reverse side if necessary and identify by block number)*
Airburst
Blast waves
Cold regions
Explosions
Shock waves

20. ABSTRACT *(Continue on reverse side if necessary and identify by block number)*

Air blast phenomena are reviewed and a digest of data is given, mainly in graphical form. To the extend possible, corresponding data are given for air blast in cold regions, provided that the prevailing conditions are significantly different from those of temperate regions.

PREFACE

This is one of a series of reports that summarize data relating to
blasting procedures and blast effects in cold regions. They are organized
to deal successively with (1) explosions in air, (2) explosions in water,
(3) explosions in solid ground materials. For the most part, the blasting
procedures used in cold regions are not much different from those that are
in general use elsewhere. Similarly, the principles involved in assessing
blast effects in cold regions are the same as those that apply to blast ef-
fects generally. The reports therefore summarize principles and data for
general explosions technology, and then present the procedures and data for
cold environments within this framework.

The purpose of the series is to provide a convenient reference source
for engineers faced with problems of explosions or blasting in cold re-
gions. Because not all engineers are well acquainted with explosions tech-
nology, relevant physical principles are explained or summarized, but there
is no attempt to explore the underlying theory in depth, nor is there any
treatment of the practical aspects of explosives use and safety practices.
These topics are covered well in Army Technical Manuals and Army Materiel
Command publications, as well as in commercial blasters' handbooks and in
textbooks.

CONTENTS :

ILLUSTRATIONS

iv

v

BLASTING AND BLAST EFFECTS IN COLD REGIONS
PART I: AIR BLAST

Malcolm Mellor

Introduction

When a shock wave propagates directly through free air, there is not
much diff rence between air blast in cold regions and air blast anywhere
else. Shock properties are influenced by differences of temperature, air
density, and atmospheric pressure, but even in temperate regions there are
large variations of temperature, pressure and density with altitude, sea-
son, and geographical location. In short, the procedures that exist for
assessing the effects of varying atmospheric conditions in temperate re-
gions are fully adequate for dealing with the conditions encountered at
high latitudes and high surface elevations.

A special feature of cold regions is widespread occurrence of snow
cover, ice-covered water bodies, hard glacial ice, and frozen ground sur-
faces. Of these, snow, and possibly floating ice, can be expected to re-
flect strong air shocks differently than hard surfaces, with consequent ef-
fects on the spatial distribution of shock properties.

The characteristic ground surfaces of cold regions can have signifi-
cantly different thermal and optical properties from those of common sur-
faces in temperate regions. This has potential significance with respect
to air blast effects from nuclear explosions, but it seems that snow, ice
and frozen ground tend to limit the effects of thermal radiation, making a
nuclear blast behave more like a conventional explosion, vi h formation of
a precursor unlikely. In other words, these surfaces are "near-ideal,"
like water, light-colored concrete, and packed soil with sparse vegetation.

Falling snow, blowing snow, and ice fog can attenuate optical and
thermal radiation from a nuclear explosion, as can rain and fog in warmer
conditions. The optical properties of all these suspensions are known in
sufficient detail for calcul   ion of the transmission and attenuation of
radiation, but this topic is outside the scope of the present report.

All of this suggests that the main requirement for understanding air blast in cold regions is a knowledge of standard air blast technology, together with some specific information on reflection and attenuation over snow surfaces.

Ideal Blast Waves in Free Air

An explosion in air forms gas at very high pressure and compresses the surrounding air, leading to expansion at supersonic speeds and to consequent formation of a shock front. If the air surrounding the explosion is homogeneous and of unlimited extent, the gas bubble expands adiabatically in a symmetric spherical pattern. Pressure at the shock front rises from ambient to a high value, called the peak overpressure, almost instantaneously. Pressure behind the shock front decreases as the gas bubble expands and changes temperature. It can drop below ambient atmospheric pressure because of inertia, and so pulsate to give secondary and tertiary pulses. As the spherical shock front expands and the pressure decreases, the shock velocity decreases until the front eventually becomes an acoustic wave.

For an observer, or a gauge, at a fixed distance from the explosion, pressure varies with time as shown in Figure 1. Between the instant of detonation and the arrival of the shock front, pressure remains at the ambient level. It then increases to a peak value almost instantaneously, and as the shock front passes the pressure decreases with time. Looking at
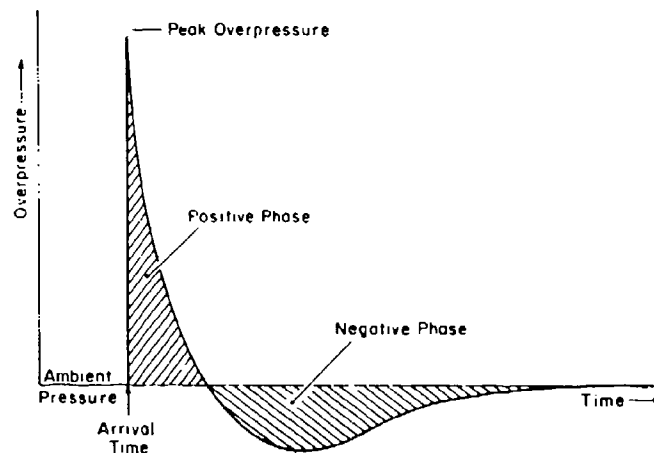
Figure 1. Variation of overpressure with time for an air shock passing a fixed observation point.

2

things another way, as in Figure 2, the pressure at any given instant is a maximum at the position of the shock front, and it decreases in the direction of the source of the explosion. If these pressure curves are plotted for successive instants, the locus of the peak pressure is the attenuation curve, i.e. the decay of peak overpressure with distance from the source. The jump in pressure across the shock front is accompanied by jumps in density, particle velocity and temperature. The variations of density and particle velocity with distance and time are qualitatively similar to the variation of overpressure as shown in Figure 2.

If the explosion is one that produces a relatively slow pressure increase, say from a gas discharge or from the burning of low explosive, the wave front near the source may have a relatively long rise time. However,
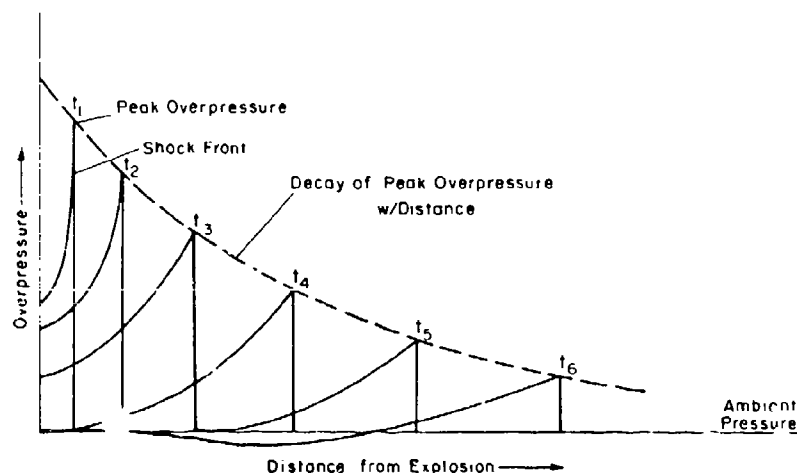
Figure 2. Variation of overpressure with distance at a given instant. Diagrams are drawn for several different times, so that the locus of peak values gives the attenuation of peak overpressure with distance.
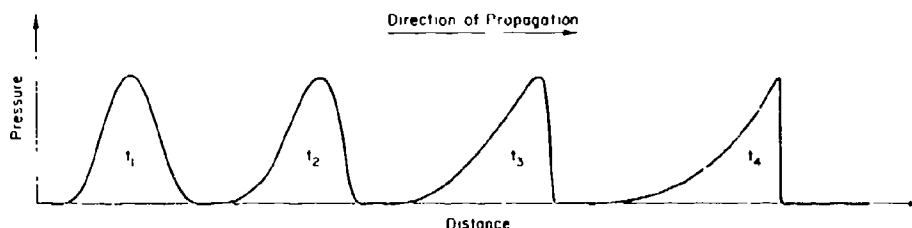
Figure 3. Change of wave form as a pressure wave with long initial rise-time steepens with time and distance so as to transform into a true shock. Attenuation is ignored in this diagram.

3

the front can steepen as it moves out, becoming a true shock at some dis-
tance from the source (Fig. 3). This effect is sometimes referred to as
"shocking up."

Overpressure is the difference between ambient pressure and pressure
behind the shock front. There is also a sort of wind pressure, called the
dynamic pressure, associated with passage of the blast wave. It is deter-
mined by air density ρ behind the shock front and by the particle velocity
u:

$$q = \frac{1}{2} \rho u^2 \tag{1}$$

where q is the dynamic pressure. When a solid obstacle is struck by air
blast, the incident and reflected overpressures of the shock front at first
dominate the loading process, producing diffraction effects and creating
vortices something like those formed by strong winds. After passage of the
shock front the dynamic pressure loads the obstacle like a wind. This
"wind" can reverse when the positive phase passes through and is followed
by the negative phase of the blast wave.

The Shock Equations for Air Blast

Shock equations can be derived for the process of detonation in an ex-
plosive, for the compression and displacement of air around an explosion
source, or for the mechanical response of any liquid or solid medium sur-
rounding an explosion. The same theory is applied in all these cases to
develop the shock relations, or Rankine-Hugoniot conditions. By consider-
ing the conservation of mass, momentum and energy across the "jump" repre-
sented by the shock front, and taking a coordinate system that travels at
the speed of the wave front (Lagrange), the following relations are ob-
tained:

Conservation of mass $\qquad\qquad u_2 \rho_2 = u_1 \rho_1 \tag{2}$

Conservation of momentum $\qquad p_2 + \rho_2 u_2^2 = p_1 + \rho_1 u_1^2 \tag{3}$

Conservation of energy $\qquad e_2 + \frac{p_2}{\rho_2} + \frac{1}{2} u_2^2 = e_1 + \frac{p_1}{\rho_1} + \frac{1}{2} u_1^2 \tag{4}$

where p, ρ, and u are pressure, density and particle velocity respectively,
and e is the internal energy. The subscripts 1 and 2 refer to conditions
on each side of the shock front. For a stationary (Euler) coordinate sys-
tem, in which the shock front travels at velocity U, the equations become:

4

$$\rho(u-U) = \rho_0(u_0-U) \tag{5}$$

$$p + \rho(u-U)^2 = p_0 + \rho_0(u_0-U)^2 \tag{6}$$

$$\rho\left(\tfrac{1}{2}u^2 + e\right)(u-U) + pu = \rho_0\left(\tfrac{1}{2}u_0^2 + e_0\right)(u_0-U) + p_0u_0. \tag{7}$$

The subscript "0" refers to ambient conditions before the arrival of the shock, and the symbols without subscripts apply immediately behind the shock. In most cases the ambient air is stationary, so that u_0 is zero.

To these mechanical conditions are added the ideal gas laws:

$$pV = p/\rho = RT \tag{8}$$

where R is the gas constant, T is absolute temperature and V is specific volume. For a polytropic gas the internal energy e is

$$e = c_v T = \frac{1}{\gamma-1} pV = \frac{1}{\gamma-1}\frac{p}{\rho} \tag{9}$$

where c_v is the specific heat at constant volume and γ is the adiabatic exponent, equal to the ratio of specific heat at constant pressure to specific heat at constant volume, c_p/c_v. For adiabatic compression or expansion

$$pV^\gamma = \frac{p}{\rho^\gamma} = A = \frac{RT}{\rho^{(\gamma-1)}} \tag{10}$$

where A is a constant. The speed of sound in the gas c is

$$c^2 = \frac{dp}{d\rho} = \gamma RT = \gamma pV = \gamma p/\rho. \tag{11}$$

Combining these relations, useful expressions for various properties of the shock front can be obtained. These expressions are given later.

Scaling Procedures for Comparison of Explosions

One of the numerous variables in explosions is the size of the charge. To simplify the comparison of explosions of different size, it is desirable to find some way to scale the variables with respect to charge size.

For a given type of explosive, pressure and detonation velocity at the source are more or less invariant with charge size, so the significant variables for the charge are energy content and physical size. If the density, specific energy and shape of the charge are constant, then charge volume and energy are directly proportional. The simplest scaling would be

5

based on geometric similitude, and this turns out to be applicable over a wide range when the given medium surrounding the explosion is homogeneous. Thus linear dimensions of the problem can be scaled with respect to a linear dimension of the charge, to the cube root of energy content, or to the cube root of charge weight. The cube root version of this scaling is sometimes referred to as Hopkinson scaling. Detailed and perceptive discussions of scaling have been given by Jones (1962) and Baker (1973).

Cube-root, or Hopkinson, scaling can be illustrated by considering the blast propagation from spherical charges of different size in an infinite homogeneous medium with unvarying properties (Fig. 4). If we are interested in the radius r at which peak overpressure has a certain value p in both explosions, then

$$\frac{r_2}{r_1} = \frac{R_{c2}}{R_{c1}} = \frac{E_2^{1/3}}{E_1^{1/3}} = \frac{W_2^{1/3}}{W_1^{1/3}} \tag{12}$$

since the energy yield of the charge E is

$$E = \frac{4}{3} \pi R_c^3 e' \tag{13}$$

and the charge weight is

$$W = \frac{4}{3} \pi R_c^3 \rho g \tag{14}$$

where e' is energy per unit volume and ρg is unit weight, both constant. R_c is the charge radius. This means that measurements of peak overpres-
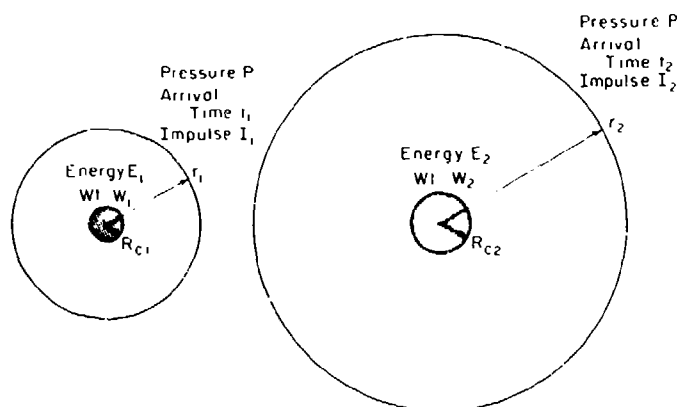
Figure 4. Scaling of shock wave properties with respect to the size and energy of the charge

6

sure p versus radius r for explosions of different size will form a single curve when p is plotted against r/R_c, against $r/E^{1/3}$, or against $r/W^{1/3}$.

Because the shock velocity U is related directly to peak overpressure, the arrival time t_a scales in the same way as radius:

$$\frac{t_{a2}}{t_{a1}} = \frac{R_{c2}}{R_{c1}} = \frac{E_2^{1/3}}{E_1^{1/3}} = \frac{W_2^{1/3}}{W_1^{1/3}} . \tag{15}$$

The positive phase duration t_p (see Fig. 1) scales in exactly the same way. Thus characteristic times for a shock front with a given pressure p are scaled as t/R_c or $t/E^{1/3}$ or $t/W^{1/3}$.

Another quantity that scales in the same way as distance and time is the impulse I, which is the integral of pressure with respect to time for the positive or negative phase of the shock. For the positive phase duration t_p,

$$I = \int_{t_a}^{t_a+t_p} (p - p_0)dt \tag{16}$$

where p is a function of time, p_0 is ambient pressure, and t_a is arrival time for the shock front. For scaling,

$$\frac{I_2}{I_1} = \frac{R_{c2}}{R_{c1}} = \frac{E_2^{1/3}}{E_1^{1/3}} = \frac{W_2^{1/3}}{W_1^{1/3}} . \tag{17}$$

Of the various scaling factors, R_c is the most attractive in the abstract, since it provides the basis for forming dimensionless variables. However, the cube root of charge weight is far more attractive for practical work, since weight is often the only thing the user knows about the charge. Figure 5 gives the conversion between "R_c scaling" and "$W^{1/3}$ scaling."

Strictly speaking, explosive type, specific energy and charge density have to be constants for scaling to apply, but in practice this is not of major importance. Among typical explosives, specific energy and density vary within a fairly narrow range, say by a factor of N, where $1.0 \leq N \leq 1.5$. For quantities scaled with respect to $E^{1/3}$, the effect on the scaling factor is $N^{1/3}$, or less than 15%.

7
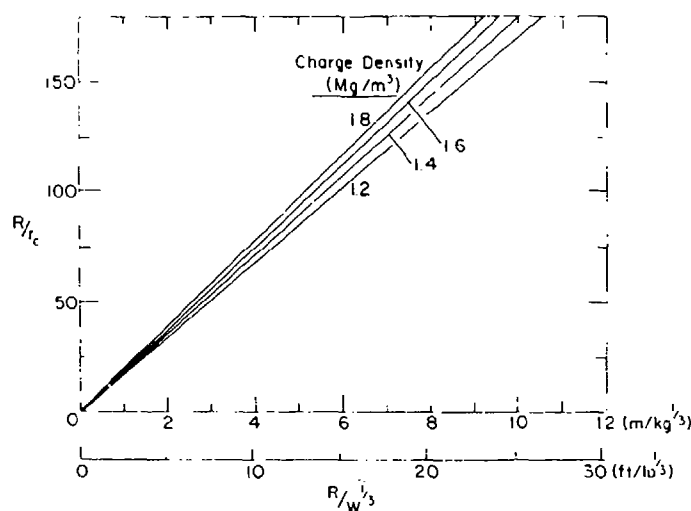
Figure 5. Conversion of scaled dimensions.
The vertical axis is length normalized with
respect to charge radius. The horizontal
axis is length scaled with respect to the
cube root of charge weight, for both tradi-
tional and SI units. The four lines give
the conversion for four different values of
charge density.

Standard curves normally use variables that are scaled with respect to
the specific energy of TNT. If the data are to be applied to explosive.,
other than TNT, or if data for other explosives are to be plotted on stand-
ard curves, a weight adjustment can be made. The equivalency factors dif-
fer according to the property considered and the medium involved. For air-
blast overpressure, equivalent weight factors are given for a range of ex-
plosives in Table 1. For comparison with nuclear explosives, W for the nu-
clear explosion is often taken as 0.5 times the radiochemical yield ex-
pressed in kilotons, i.e. 1 kiloton would be equivalent to 10^6 lb of TNT
for generation of airblast overpressure.

If the ambient pressure of the homogeneous atmosphere is different for
different explosions, a different set of scaling relations is used. In
this scheme, known as Sachs scaling, dimensional analysis is used to derive
normalizing parameters which make the blast properties and distances dimen-
sionless. In particular, overpressure and dynamic pressure are normalized
with respect to the ambient air pressure p_0, and distance is scaled with
respect to the quantity $(E/p_0)^{1/3}$, where E is the energy yield of the
charge. As was mentioned earlier, E is proportional to the charge weight
W, so that for working purposes $(E/p_0)^{1/3}$ can be replaced by $(W/p_0)^{1/3}$.

8

Table 1. Equivalent weight factors for comparing air blast overpressures. Data from Swisdak (1975).

Explosive	Equivalent weight relative to TNT
Composition A-3	1.09
Composition B	1.11
Composition C-4	1.37
Cyclotol (RDX/TNT 70/30)	1.14
HBX-1	1.17
HBX-3	1.14
H-6	1.38
Minol II	1.20
Octol (HMX/TNT 70/30 and 75/25)	1.06
PETN	1.27
Pentolite	1.42
Pentolite (high overpressure)	1.38
Picratol	0.90
Tetryl	1.07
Tetrytol (Tetryl/TNT 75/25, 70/30, 65/35)	1.06
TNETB	1.36
TNT	1.00
Tritonal	1.07
ANFO (AN/FO 94/6)	0.82
PBX-9404	1.13
PBX-9010	1.29
Nitroglycerin Dynamite (50%)	0.9
Ammonia Dynamite (50%)	0.9
Ammonia Dynamite (20%)	0.7
Gelatin Dynamite (50%)	0.8
Gelatin Dynamite (20%)	0.7

Note: Comparisons made for overpressures mostly in the range 5-100 $lbf/in.^2$ (0.03 to 0.7 MPa).

With Sachs scaling, characteristic times (e.g. arrival time, phase duration) are scaled with respect to the quantity $(E/p_0)^{1/3} (1/c_0)$, where c_0 is the acoustic velocity of the ambient air. Velocities are scaled with respect to c_0. Impulse is scaled with respect to $(E/p_0^2)^{1/3}/c_0$. In all cases, distances are scaled with respect to $(E/p_0)^{1/3}$, so that scaled distance varies with the ambient pressure. Sachs scaling applies over the range of distances where the air behaves as an ideal gas.

9

It is not intended for use very close to the explosion source, where peak overpressure is of order 10^3 lbf/in.^{2} (7 MPa) or greater.

Standard values of p_0, c_0, and the reference values of density and temperature are given in Figure 44.

Reflection and Refraction of Airblast

When a large explosion occurs at low altitude, the spherical shock front travels downward and outward until it impinges on the ground surface and reflects.

The reflection of acoustic waves and weak shocks from a rigid surface is analogous to reflection in optics (Fig. 6a). Regular reflection occurs, with the angles of incidence and reflection equal, and at the reflecting surface the pressure of the incident wave doubles. Natural ground surfaces are often porous and/or deformable, permitting some wave penetration and energy transfer to the ground. This can give reflection that is out of phase with the incident wave.

Directly below the source of a strong shock there is also a region of regular reflection, but the angles of incidence and reflection are not equal, and the reflected wave is not perfectly spherical (Fig. 6b). The

a. Regular reflection of acoustic waves   b. Reflection of strong shocks,
and weak shocks.   with Mach stem formation.
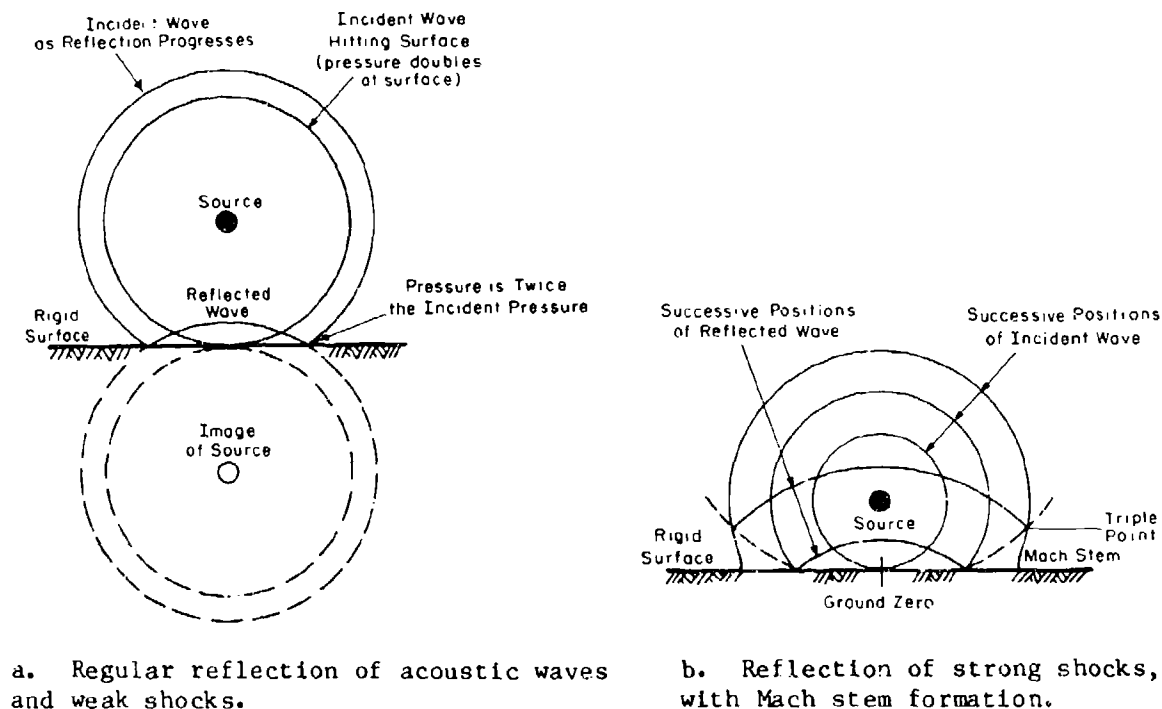
Figure 6. Reflection of shock waves at a rigid surface.

10
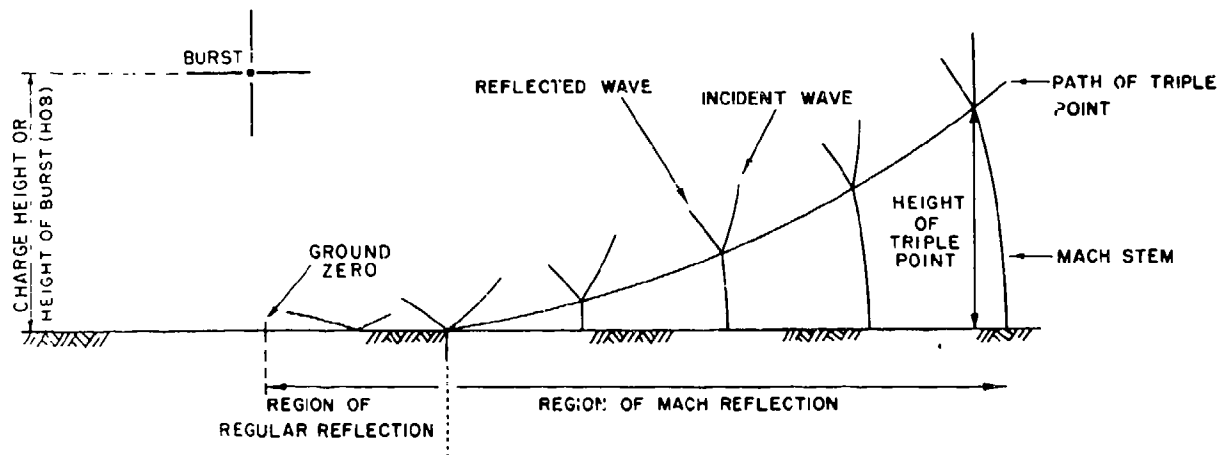
Figure 7. Reflection of the shock wave from an air burst and formation of the Mach stem.

complications arise from the fact that the air behind the incident shock is at higher pressure, density and temperature than the free air through which the incident wave traveled. Thus the reflected wave travels in a medium with different, and spatially varying, properties. As a result, its velocity and pressure are affected. The pressure amplification in a normally reflected wave is much more than the factor of 2 that applies in weak shocks and elastic waves; the amplification factor could be in the range 8 to 20 for reflection from "hard" surfaces (Baker 1973; see also Fig. 15). A pressure transducer located in air within the region of regular reflection experiences two separate shocks, one as the incident wave passes "outward bound," and a second as the reflected wave returns.

The reflected shock travels faster than the incident shock and, in the region where oblique reflection occurs, the reflected shock can catch up with the incident shock, fusing with it to form a single front, called a Mach front. As the shock front expands, the size of the fused zone increases and the height of the Mach stem increases with distance from ground zero (Fig. 7).

The locus of the triple point, shown schematically in Figure 7, is given quantitatively for a range of charge heights in Figure 8, using scaled variables.

So far, the air has been assumed homogeneous. However, for large explosions the earth's atmosphere is not homogeneous, but rather is layered. The effective velocities of sound waves and shock waves vary with altitude,
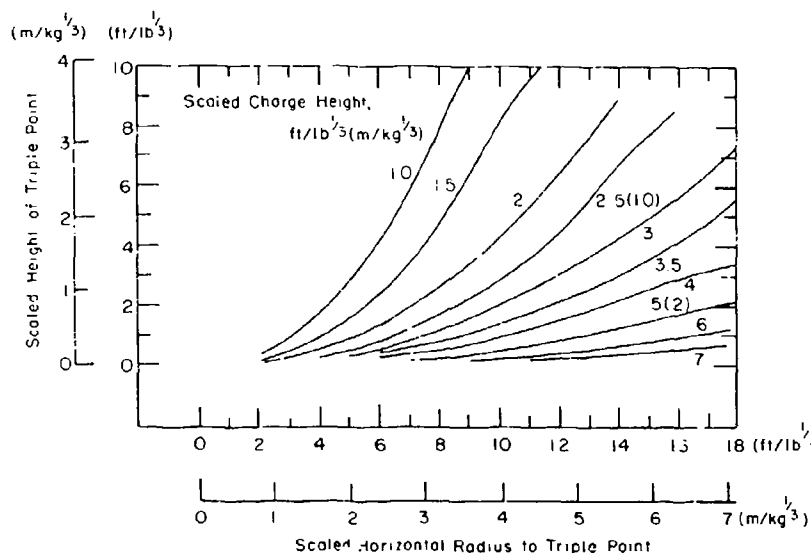
Figure 8. Height of triple point (or Mach stem) as a function of horizontal radius from the burst axis to the triple point. Curves are given for various charge heights. All linear dimensions are scaled with respect to the cube root of charge weight.
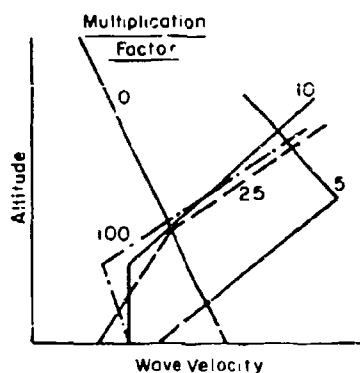
Figure 9. Approximate magnitude of reinforcement for ground level air blast focused at long range by atmospheric conditions. The graphs represent vertical profiles of wave velocity. The number on each graph is a representative multiplication factor for the type and intensity of the velocity profile. After Baker (1973).

largely because of changes in temperature and wind speed. From eq 11, acoustic velocity is proportional to the square root of absolute temperature, i.e. $c = (\gamma R)^{1/2} T^{1/2}$. Wind does not affect c of itself, but it changes the velocity relative to the stationary ground surface (see eq 18 below). If wave velocity increases with altitude, waves are refracted and turned back towards the ground surface. This can be thought of as analogous to refraction and internal reflection of rays in optics. The reinforcement of ground level air blast from such effects is referred to, sometimes loosely, as focusing. At certain "focus" distances from an explosion, ground level air blast can be multiplied by factors up to 100 by vertical wave velocity gradients of various types and intensities (Fig. 9).

12

The atmospheric factors controlling air blast can best be appreciated by considering simplified conditions. In the unlikely event of perfectly calm conditions with no vertical gradient of temperature, the acoustic velocity is uniform and the wave front from an explosion propagates in a perfectly spherical pattern. Thinking in terms of "rays" that are orthogonal to the wave front, this condition gives straight rays radiating out from the explosion source (Fig. 10a). A much more likely situation is one where the temperature, and therefore the acoustic velocity, decreases with increase of altitude at a characteristic gradient (adiabatic lapse rate). In this case, the wave front is distorted from the perfect spherical pattern and the "rays" are bent in an upward direction (Fig. 10b). This condition tends to funnel shock and noise upward, reducing overpressure and noise at ground level for long ranges. With the opposite condition (an increase of temperature and acoustic velocity with increasing height) the wave front speeds up as it rises, causing the "rays" to bend downward (Fig. 10c). This increase of temperature with height, known as a temperature inversion, often develops in the lowest layers of the atmosphere as a result of overnight cooling in calm weather. Air blast at ground level can increase considerably when a temperature inversion exists, and so this situation is unfavorable for commercial blasting in populated areas. Large explosions give significant air blast effect up to high altitudes, and in these circumstances it is unlikely that there will be a uniform temperature gradient in the atmosphere. With discontinuities and reversals in the gradient of acoustic velocity, the ray paths, interferences, and reflections can become complicated. At ground level, there may be zones of relative silence, and zones where the blast is intensified. Figure 10d gives an example of a condition where the velocity gradient reverses.

Another factor is wind, which has both direct and indirect effects. The direct effect is that sound waves travel in moving air, so that the effective velocity relative to the ground (c') is the vector sum of acoustic velocity c and the wind velocity u:

$$c' = c + u \cos\theta \tag{18}$$

where θ is the azimuth from the downwind direction. u varies with height, typically because of wind shear against the ground surface, so that c' also varies with height. The indirect effect comes from the influence of wind on the temperature profile. Direct wind effects are similar to temperature

13
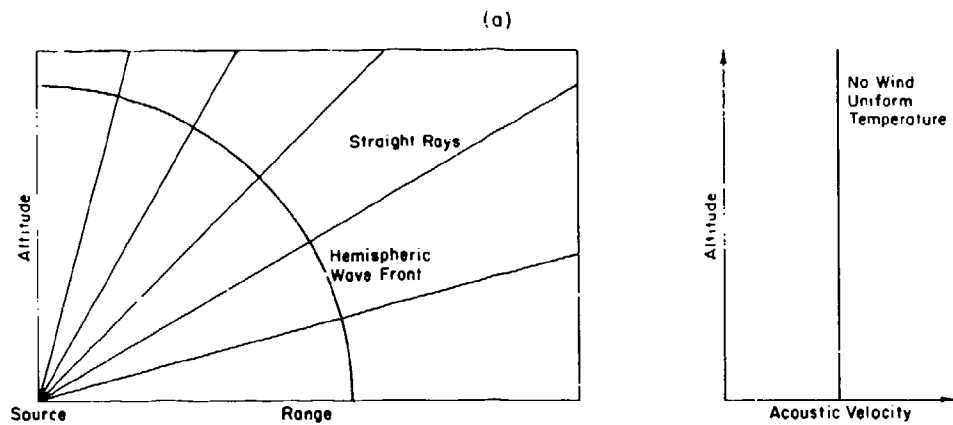
a. Undistorted propagation with zero gradient of acoustic velocity.
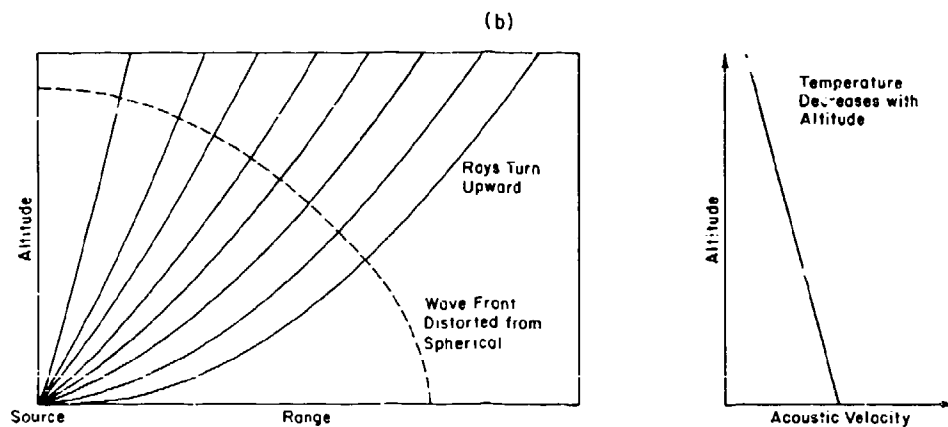
b. Upward deflection when acousti~ velocity decreases with altitude.
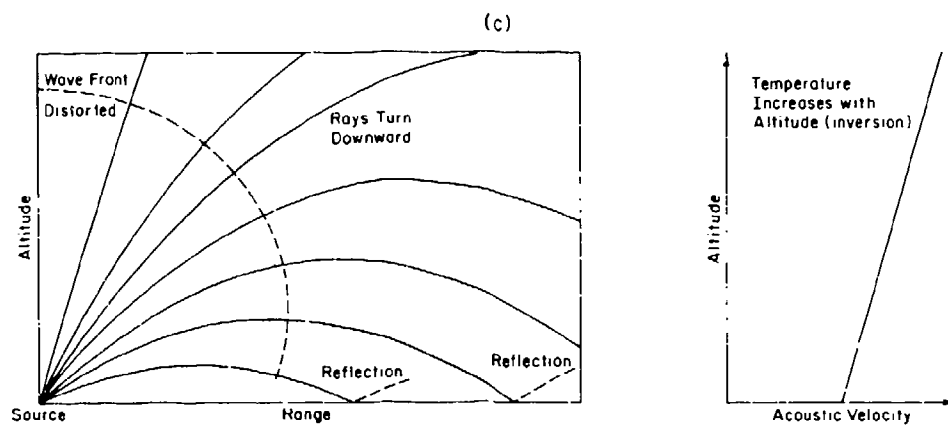
c Downward deflection when acoustic velocity increases with altitude.

Figure 10. Refraction of air waves by vertical gradients of acoustic velocity.

14
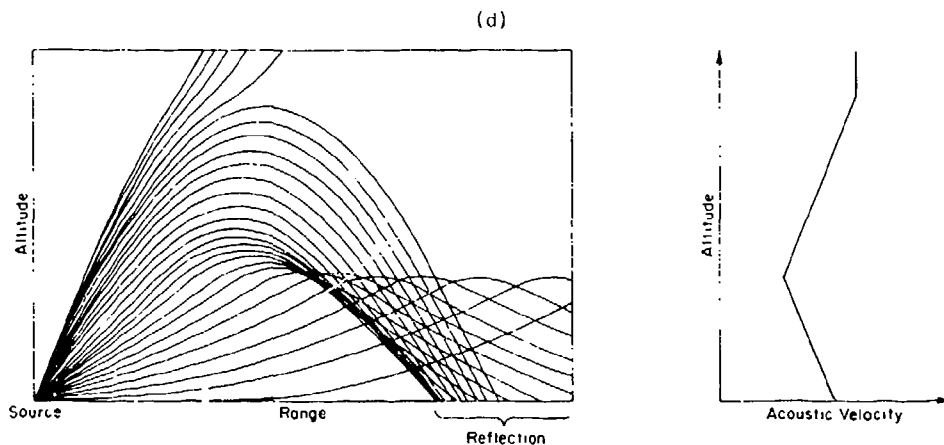
d. Deflection and interference with stratification and reversal
of velocity gradients.

Figure 10 (cont'd).
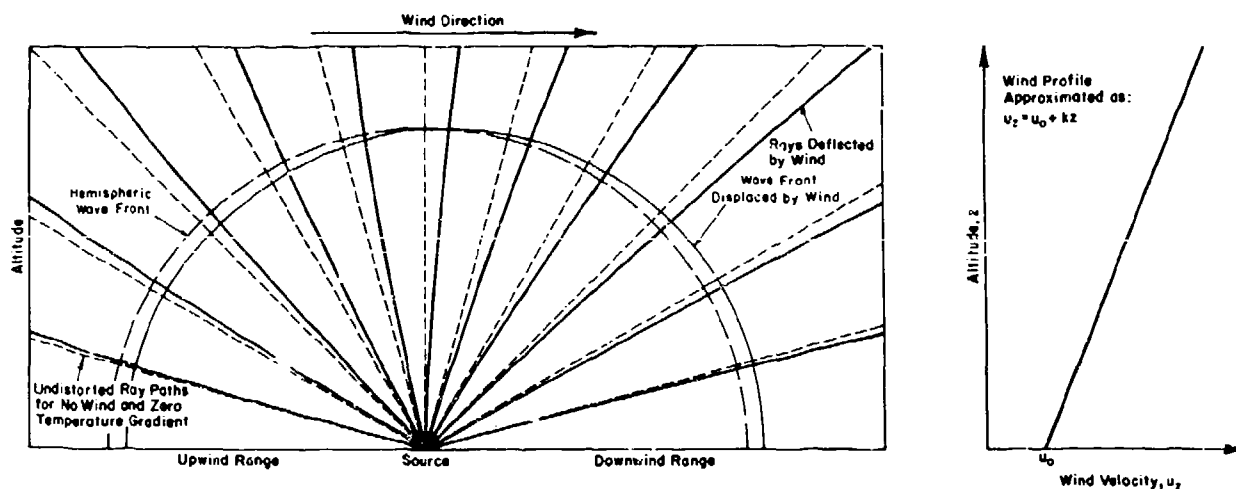
Figure 11. Effect of wind on air wave propagation. In the lower atmosphere,
rays tend to be bent slightly by a gradient of wind velocity.

effects, given corresponding profiles of acoustic velocity. However, while
temperature effects are omnidirectional, wind effects vary in azimuth.
With a typical surfac wind profile, rays downwind of the source tend to
refract downward, while rays upwind of the source tend to bend upwards.
Figure 11 shows how blast rays would be affected by wind alone, i.e. how
they would deflect with wind speed increasing with altitude, but with air
temperature uniform.

Effect of Charge Height, or Height of Burst

When a charge is fired close to the surface, che attenuation of over-pressure with horizontal distance is similar to the attenuation with radius in free air. However, when the charge i high above the surface, the over-pressure experienced at ground level is attenuated by both downward travel and outward travel, i.e. it decreases as a function of the slant range. This means that as the horizontal radius from ground zero decreases to zero, the peak overpressure tends to a limit at moderate pressure levels, instead of increasing to very high values as it would if the charge were close to the surface. As the charge height increases, the peak ground level overpressure near ground zero also decreases. However, the ground level overpressure at large scaled radii is not much affected. Figure 12 gives a set of pressure contours which shows how the peak overpressure at
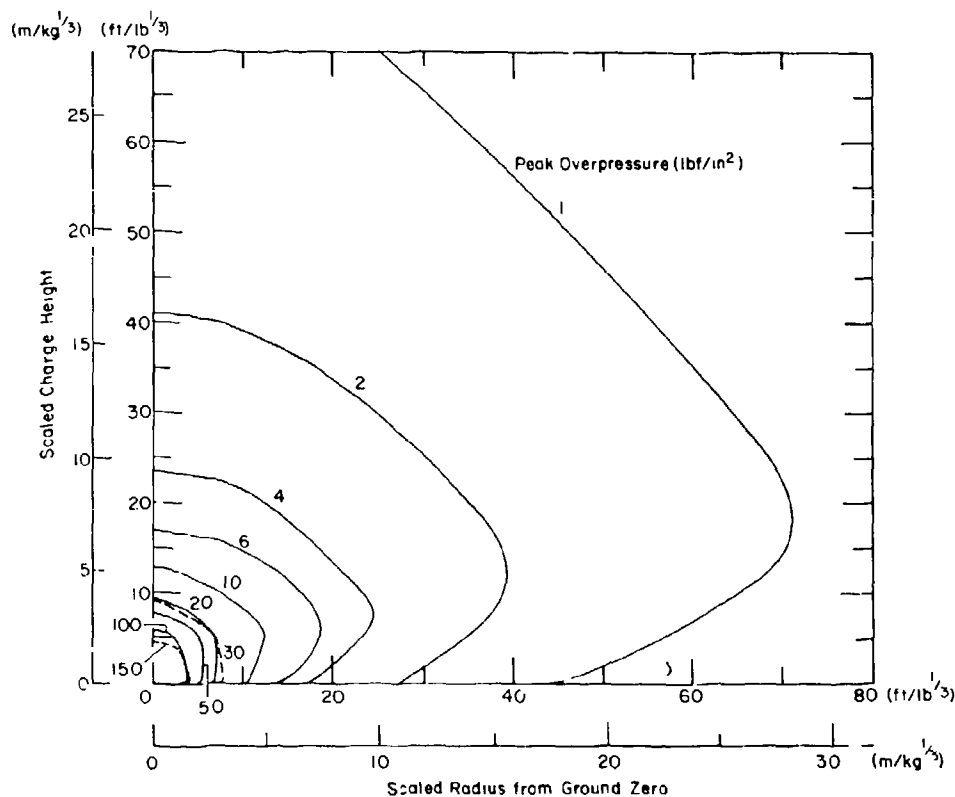
Figure 12. Effect of charge height and ground level radius on peak overpressure. Contours are for even values in lbf/in.[2] For conversion to bars, multiply by 0.06895. For conversion to kPa, multiply by 6.895. Data from Swisdak (1975).

16
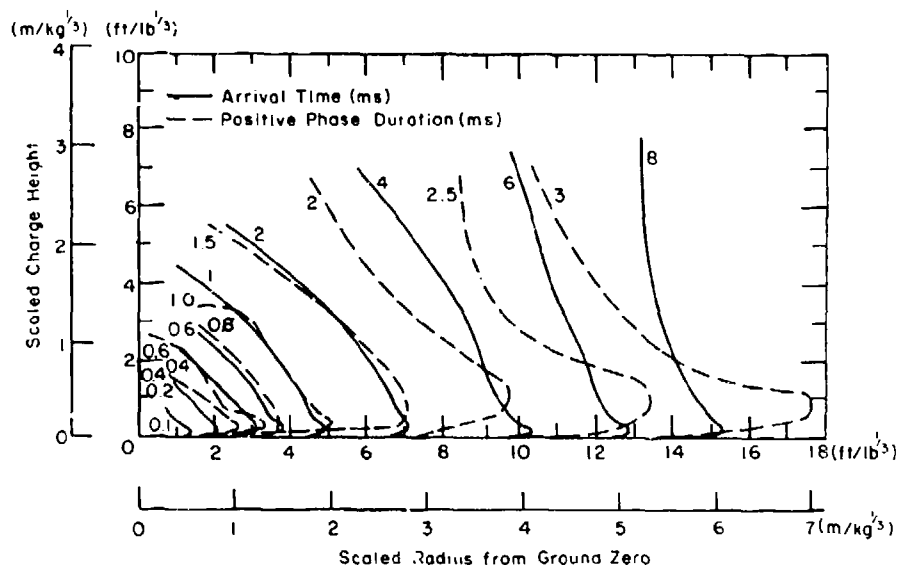
Figure 13. Effect of charge height and ground level radius on the arrival time and the positive-phase duration. Data from Swisdak (1975).
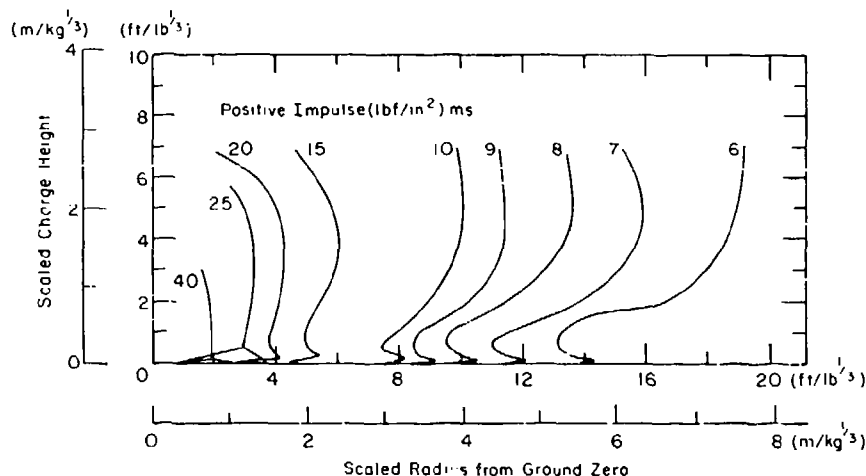
Figure 14. Effect of charge height and ground level radius on the positive impulse. The curves are drawn for given levels of impulse in $(lbf/in.^2)ms$. To convert to $(bars)ms$ or $(kPa)ms$, multiply the values by 0.06895 or 6.895 respectively. Data from Swisdak (1975).

ground level varies with scaled radius from ground zero and with scaled charge height.

The arrival time and the positive phase duration at ground level are also affected by the charge height. The general pattern of variation is shown in Figure 13.

Corresponding data for the positive impulse are given in Figure 14.

17

Attenuation of Air Blast and Variation of Shock Front Properties

As a blast wave spreads from the source, it attenuates. The peak overpressure, the dynamic pressure, the shock velocity and the peak particle velocity all decrease with increasi g distance from the source. The density and temperature of the air behind the shock front also decrease with increasing radius. The positive phase duration shows an overall increase with increasing radius, while the impulse of positive overpressure has an overall decrease as radius increases. Figures 15-18 illustrate the variation of shock properties with radius by means of dimensionless graphs based on Sachs scaling.
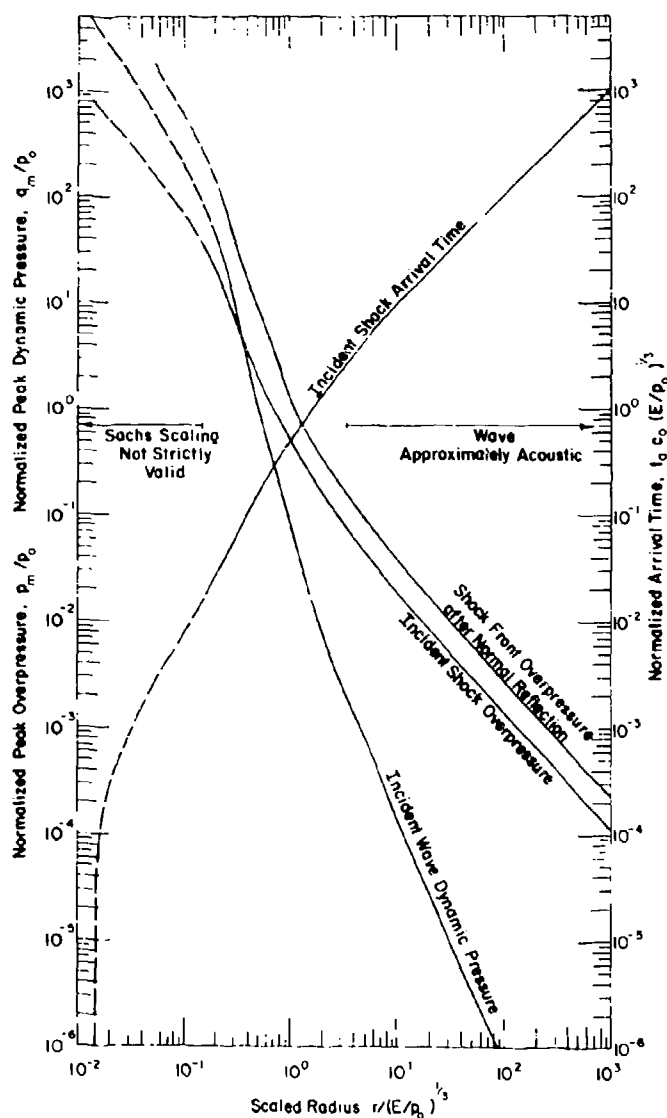
Figure 15. Dimensionless (Sachs) plot of peak overpressure, peak dynamic pressure, and arrival time, all as functions of radius. From data compiled, selected and adjusted by Baker (1973).

18
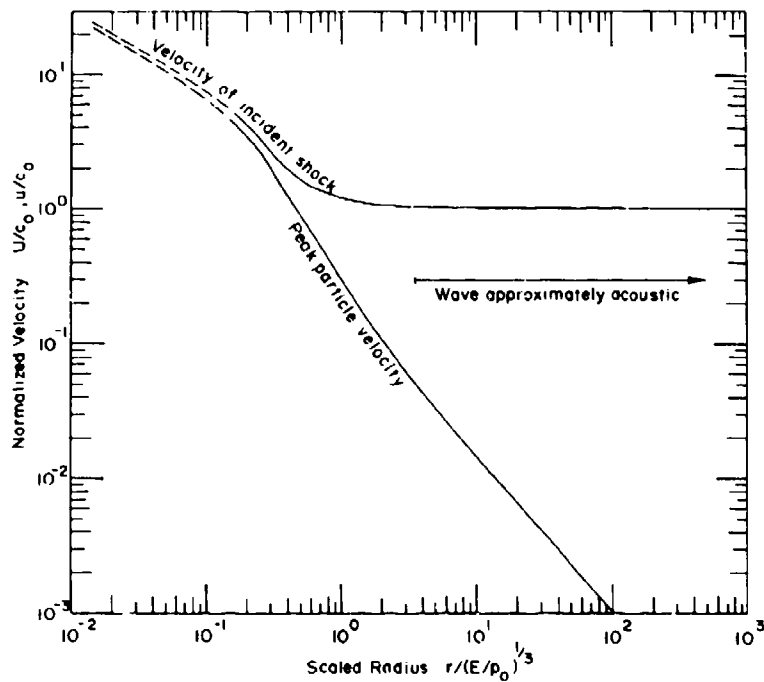
Figure 16. Dimensionless (Sachs) plot of shock vel-
ocity and peak particle velocity as functions of
radius. From data compiled, selected and adjusted
by Baker (1973).
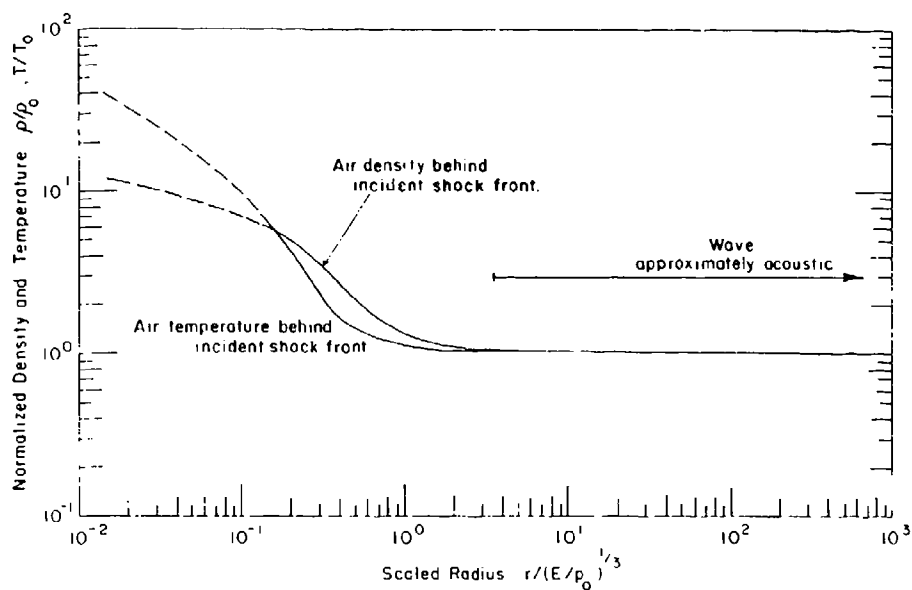
Figure 17. Dimensionless (Sachs) plot of air density and air
temperature as functions of radius. From data compiled, se-
lected and adjusted by Baker (1973).

19
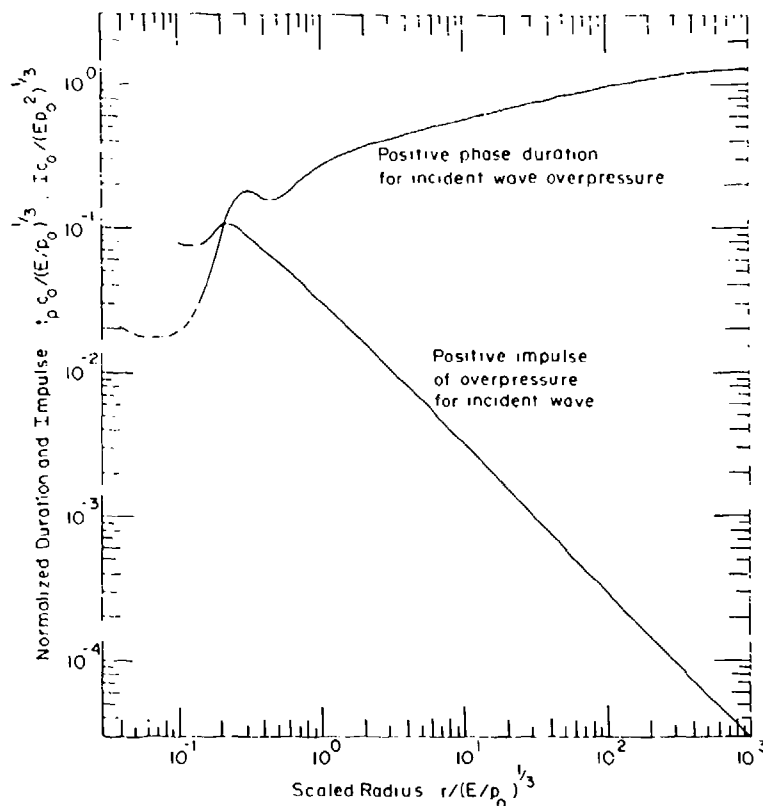
Figure 18. Dimensionless (Sachs) plot of positive phase duration and positive impulse as functions of radius. From data compiled, selected and adjusted by Baker (1973).

Close to a concentrated source, the attenuation of overpressure p_m should be rapid. Taylor's (1950) solution of the equations for spherical strong shocks predicts an inverse cube decay, i.e. $p_m \propto 1/r^3$. By contrast, at long distances from the explosion the air blast has slowed down to become an acoustic (elastic) wave, so that the peak pressure should be inversely proportional to distance, i.e. $p_m \propto 1/r$. Figure 19 gives a representative curve for the variation of peak overpressure with distance in free air. To avoid complications from inhomogeneity of the ambient air and from surface reflections, it is necessarily based on data for small charges of high explosive, which have finite size. The broken line for high pressure at close range represents the effect of finite source diameter; for a true point source, the close-range attenuation should follow an inverse cube trend.

20
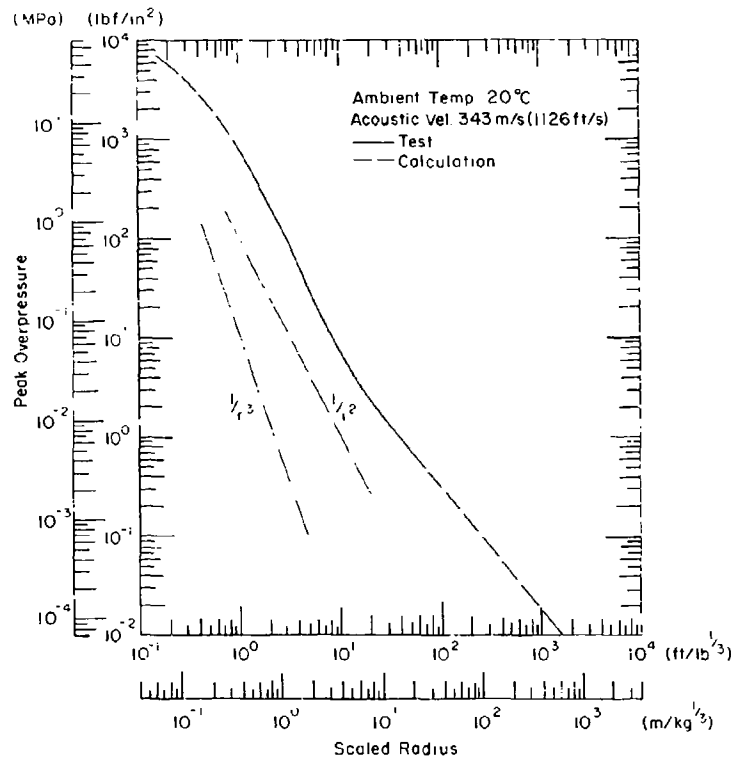
Figure 19. Representative attenuation curve for high explosive charges in "homogeneous" free air. From tabulated unscaled data and calculated extensions of curve, as given by Swisdak (1975). Checked against other field test data for limited ranges.

In typical practical problems the main concern is with air blast propagated at ground level from a charge that detonates near ground level. The overpressure experienced is that produced after reflection and wave fusion, as described earlier. To remove variability due to charge height (height of burst), data have been collected for surface bursts of various sizes. Test results are not completely identical when presented in scaled form, but Figure 20 gives a representative curve for the attenuation of peak overpressure with scaled distance at sea level (the upper limit of the band represents a 1-kiloton nuclear burst at sea level). Comparing Figures 19 and 20, it can be seen that the curves for free air and for surface propagation are not much different. It can also be seen that the data do not support the point-source prediction of inverse cube decay ($p_m \propto 1/r^3$). In the region where peak overpressure is from 10 to 1000 lbf/in.^{2} (70 kPa to 7 MPa), an inverse square decay ($p_m \propto 1/r^2$) is a better approximation.

21
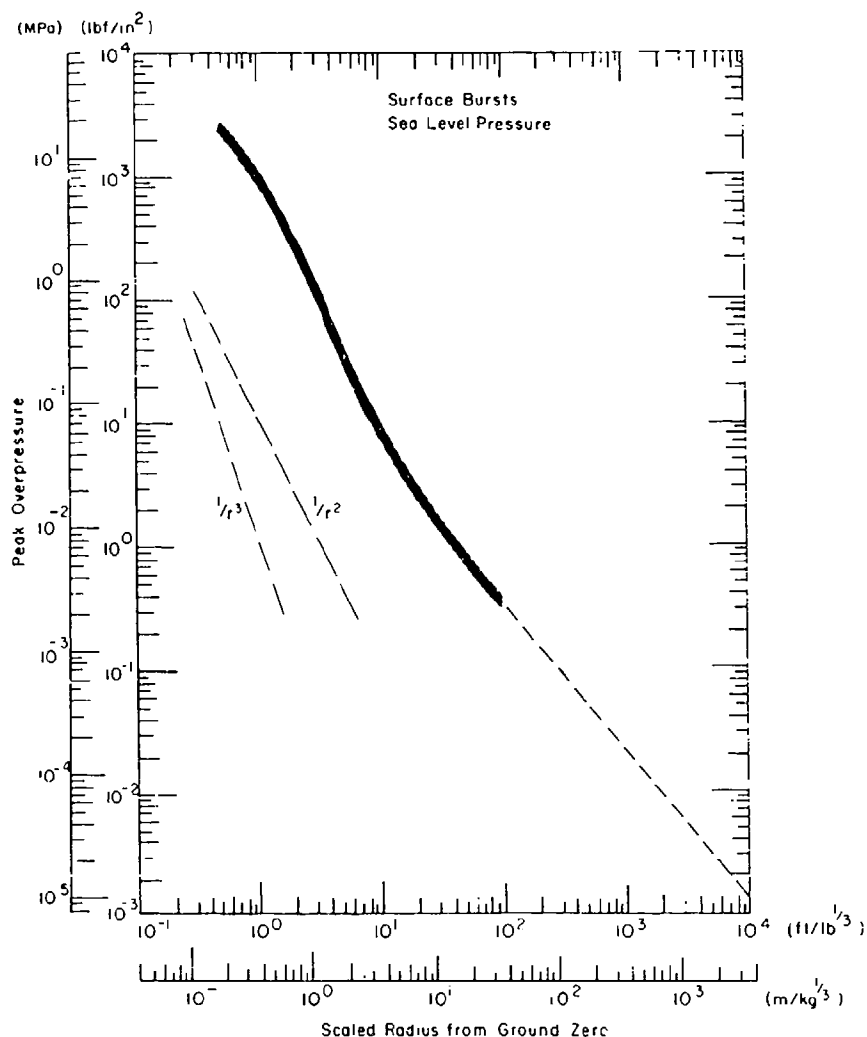
Figure 20. Representative attenuation curve for ground-level overpressure from contact and near-surface bursts. HE and nuclear data from various sources (see Swisdak 1975, Baker 1973, Glasstone 1962, Defense Nuclear Agency 1972, U.S. Army 1984, du Pont 1977).

Arrival time and phase duration. Arrival time and phase duration both scale with respect to the cube root of energy or charge weight (eq 15). Figure 21 gives representative curves for a small explosion in free air. They can be used as follows: (1) for a given actual distance, obtain the scaled distance by dividing by the cube root of charge weight, (2) for this scaled distance, read off the scaled time, (3) convert the scaled time to actual time by multiplying by the cube root of charge weight.

22
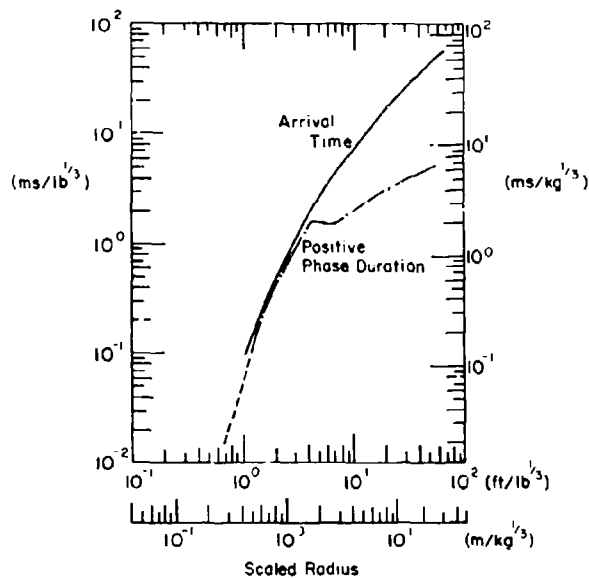
Figure 21. Variation of arrival
time and positive-phase duration
with radius for an explosion in
free air. From Swisdak (1975).

Air blast impulse. The impulse from the positive phase of the shock
wave is defined by eq 16 and scaled relations for impulse are given in eq
17. As a very rough approximation, the pressure/time plot for the positive
phase is a triangular figure, so that the impulse at any given distance
from the source is roughly proportional to the product of peak overpressure
(Fig. 20) and phase duration (Fig. 21). Figure 22 gives the approximate
magnitude of scaled positive impulse as a function of scaled radius for

Figure 22. Variation of positive impulse with
radius for surface bursts and free air bursts.
Adapted from Swisdak (1975).

23

surface bursts and for propagation in free air. Scaled values of impulse are converted to actual values by multiplying by the cube root of charge weight.

Dynamic pressure. If the air behind the shock front behaves as an ideal gas, the dynamic pressure q can be expressed as a function of the overpressure p:

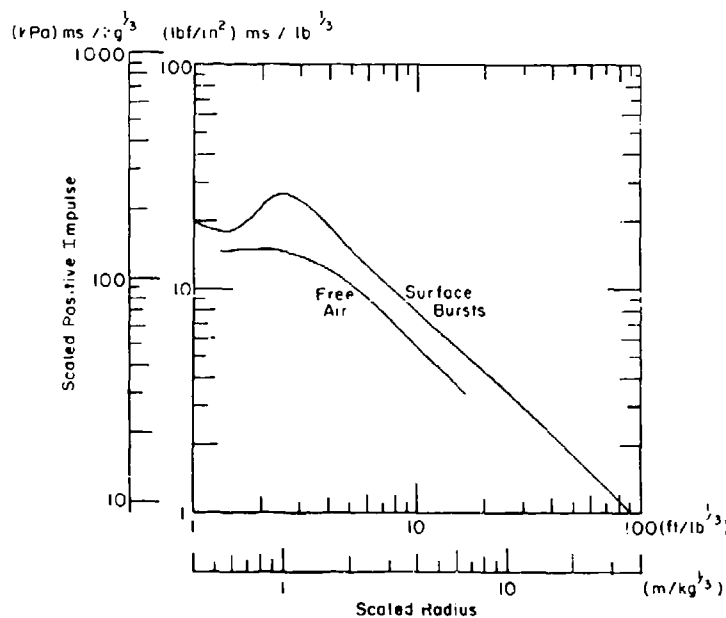$$q = \frac{p}{(\gamma-1) + 2\gamma (p_0/p)} \approx \frac{p}{0.4 + 2.8 (p_0/p)} \tag{19}$$

where p_0 is ambient pressure and γ is the ratio of specific heats, usually taken as 1.4 for air. If this relation is accepted, the attenuation of peak dynamic pressure q is determined by the attenuation relation for peak overpressure p. Equation 19 is probably acceptable for surface bursts when the scaled radius exceeds about 2 ft/lb$^{1/3}$, or 0.8 m/kg$^{1/3}$.

Particle velocity. The particle velocity u can also be expressed in terms of overpressure p and ambient pressure p_0 by using the shock equations and the gas laws:

$$u = \frac{c_0}{\gamma} \cdot \frac{p}{p_0} \left(1 + \frac{\gamma+1}{2\gamma} \cdot \frac{p}{p_0}\right)^{-1/2}$$

$$\approx \frac{0.714 c_0 (p/p_0)}{[1 + 0.957(p/p_0)]^{1/2}} \tag{20}$$

where c_0 is acoustic velocity in ambient air ahead of the shock and γ is taken as 1.4.

Shock Velocity. The theoretical relation between shock velocity U and peak overpressure p is

$$U = c_0 \left(1 + \frac{\gamma+1}{2\gamma} \cdot \frac{p}{p_0}\right)^{1/2}$$

$$\approx c_0 \left[1 + 0.857 (p/p_0)\right]^{1/2}. \tag{21}$$

Actual values of shock velocity can be obtained from test data for arrival time, as shown in Figure 21. The shock velocity U at a scaled radius $\bar{r}$ is

$$U = \frac{d\bar{r}}{d\bar{t}} \tag{22}$$

where $\bar{t}$ is scaled arrival time at scaled radius $\bar{r}$.

24

Air density behind the shock front. Air density behind the shock
front, ρ, is related to the peak overpressure p by

$$\frac{\rho}{\rho_0} = \frac{1 + [(\gamma+1)/2\gamma]p/p_0}{1 + [(\gamma-1)/2\gamma]p/p_0}$$

$$\approx \frac{1 + 0.857 \; p/p_0}{1 + 0.143 \; p/p_0} \tag{23}$$

where ρ_0 is air density ahead of the shock.

Reflected pressure. The shock equations and gas laws give a theoreti-
cal value for the reflected presure p_r at the instant when the incident
shock strikes a flat, rigid surface at normal incidence:

$$p_r = 2p + (\gamma+1)q$$

$$= p\{\frac{4\gamma + (3\gamma-1)p/p_0}{2\gamma + (\gamma-1)p/p_0}\}$$

$$\approx 2p(\frac{7 + 4 \; p/p_0}{7 + p/p_0}) \tag{24}$$

where p is the incident peak overpressure.

Glasstone (1962) noted that for very high values of the incident peak
overpressure p, the reflected overpressure tends to a limit of $p_r = 8p$.
However, Baker (1973) pointed out that the ideal gas assumption is probably
not justified for very high temperatures and pressures, citing studies that
suggest p_r/p can be as high as 20 or more for very intense shocks.

Figure 23 shows graphically the variations of dynamic pressure, parti-
cle velocity, shock velocity, air density and reflected pressure with peak
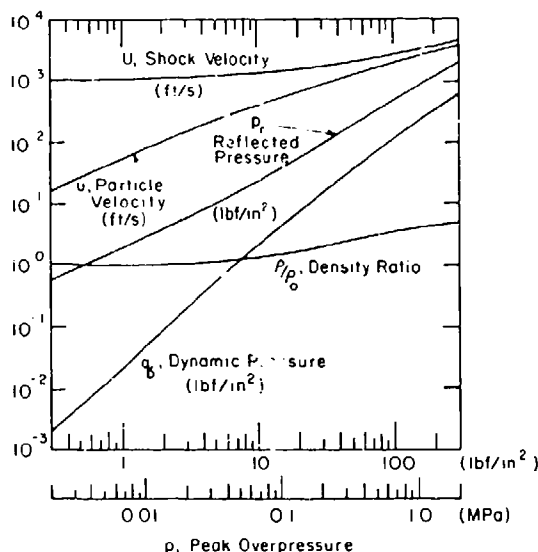

Figure 23. Variation of shock
properties with peak overpres-
sure. From Swisdak (1975).

25

overpressure. The range of p is limited in the graph to a range where the ideal gas assumption is likely to be justifiable.

Air Blast from Nuclear Explosions

In general, nuclear explosions are on a bigger scale than chemical explosions, and the units used for scaled dimensions are based on a kiloton of yield* rather than on a pound or kilogram of high explosive. The very large scale of the blast means that the atmosphere is influenced over a large range of altitude, so that vertical gradients of density and temperature are important. Another difference is that nuclear explosions emit intense thermal radiation, while thermal radiation from typical high explosives is negligible. Thermal radiation absorbed by the ground surface causes heating and the formation of a precursor shock.

A nuclear contact burst is defined as a nuclear explosion in air at scaled heights from zero to 5 ft/kt$^{1/3}$ (1.5 m/kt$^{1/3}$). It produces a shock front that is approximately hemispherical. An air burst at higher level, say from 5 to 160 ft/kt$^{1/3}$ (1.5 to 50 m/kt$^{1/·}$) propagates an approximately spherical shock, which reflects on contact with the surface, as described previously for high explosives (p. 7). A Mach stem is formed by fusion of the incident and reflected shocks, and air motion behind the Mach stem produces a second shock (Fig. 24). Ahead of the Mach stem, heating of
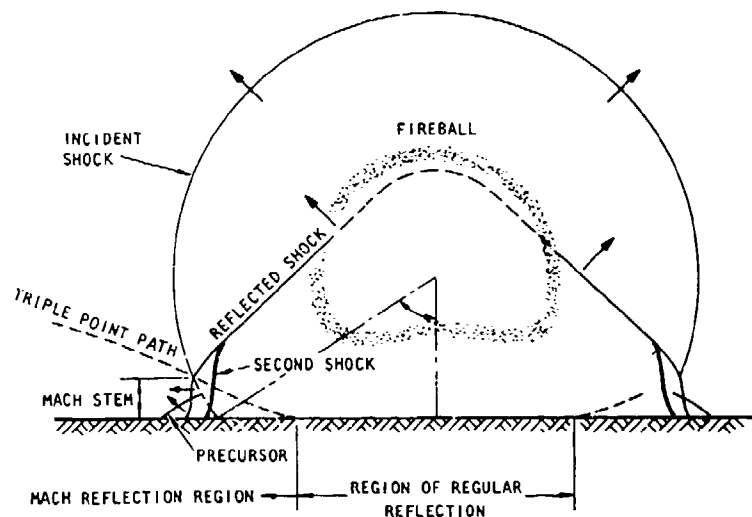
Figure 24. Shock geometry for the air blast of a nuclear explosion (Brode 1964, U.S. Army 1984).

* Abbreviated "kt."

the ground by thermal radiation causes the formation of a precursor wave near the surface (Fig. 24). The amount of heating produced by thermal radiation varies with the reflectance, or albedo, of the ground surface, and with the thermal properties of the surface materials. Ground surfaces are classified as either "thermally near-ideal" or "thermally non-ideal"; the former are unlikely to create a precursor, but a precursor can occur over the latter. Table 2 gives examples of these two types.

Representative distribution of peak overpressure is shown in Figure 25 for surfaces that are near-ideal. Over surfaces that are thermally non-ideal, overpressure contours are distorted in the zone of Mach reflection out to a radius of 1500 $ft/kt^{1/3}$ (460 $m/kt^{1/3}$), or to the 6-$lbf/in.^2$ contour.
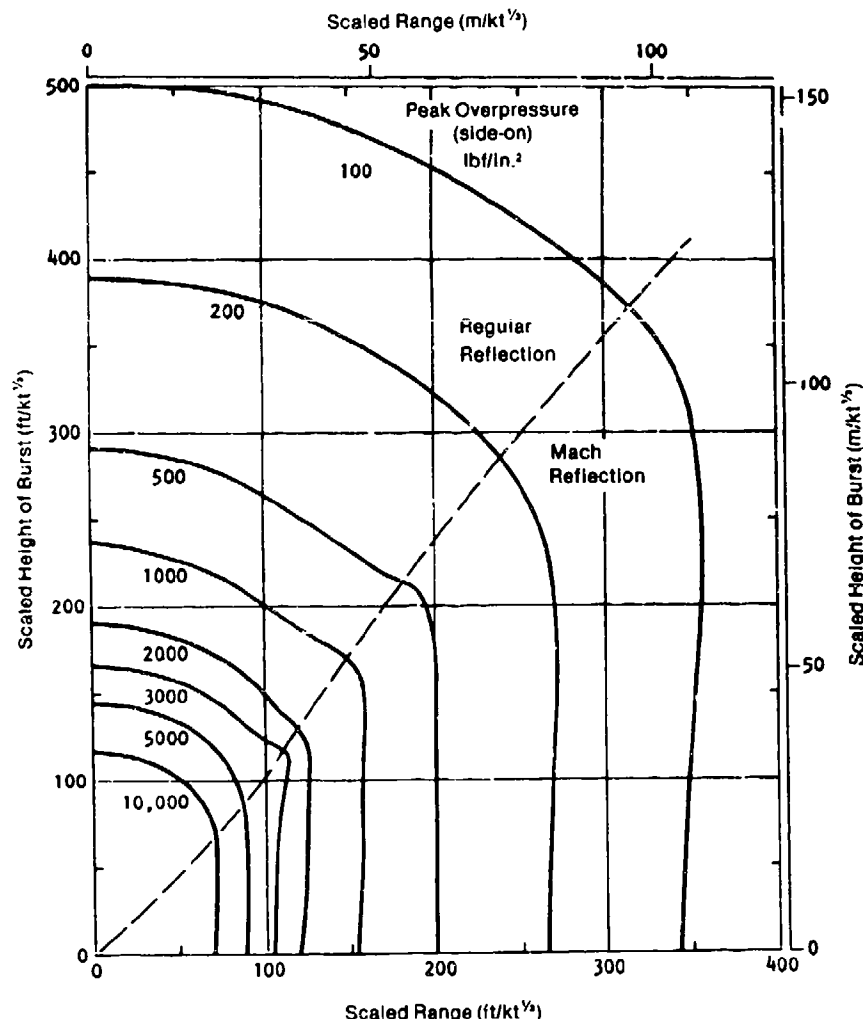
a.   Very high overpressures at close range.

Figure 25.   Variation of peak overpressure with charge height and horizontal radius for a near-ideal surface subjected to a nuclear explosion (U.S. Army 1984, DNA 1972).

27
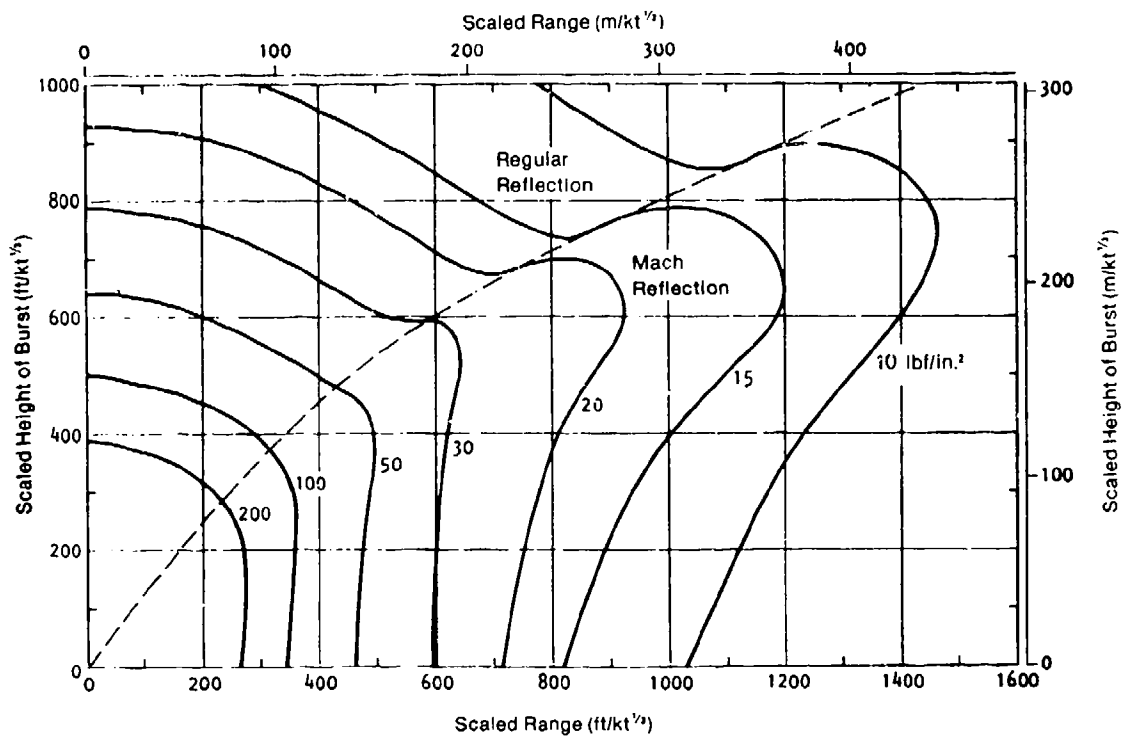
b. High overpressures extending further from ground zero.
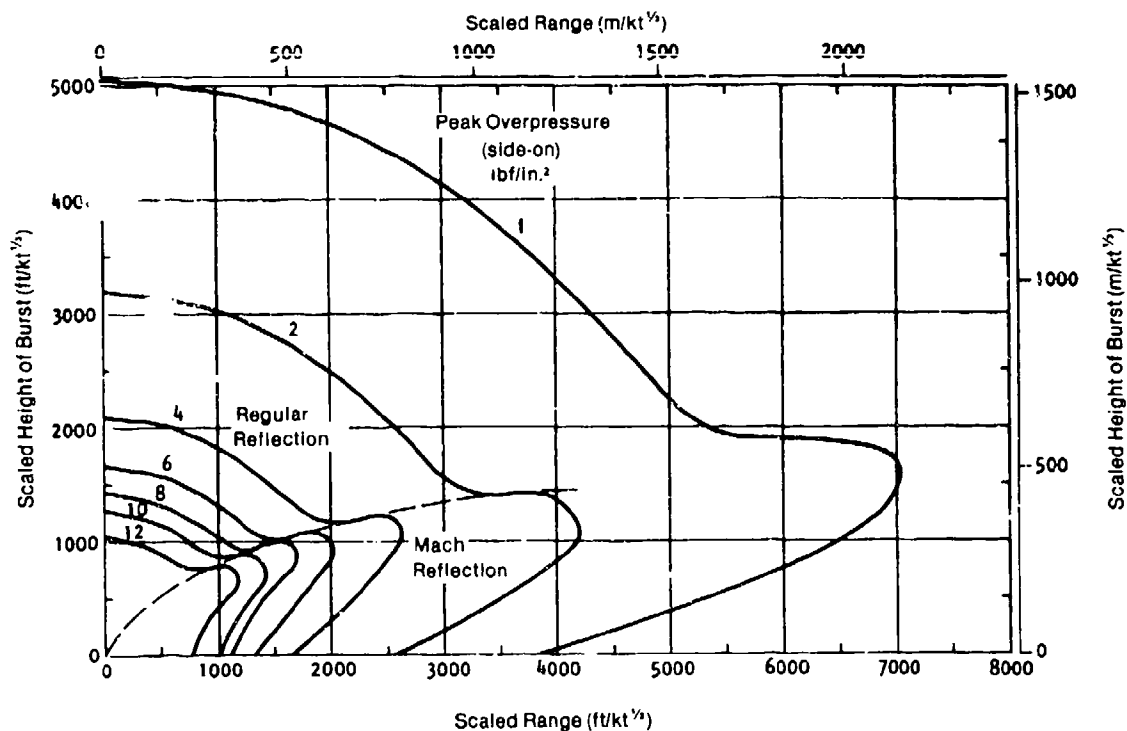
c. Low overpressures at appreciable distances from the explosion.

Figure 25 (cont'd). Variation of peak overpressure with charge height and horizontal radius for a near-ideal surface subjected to a nuclear explosion (U.S. Army 1984, DNA 1972).

28
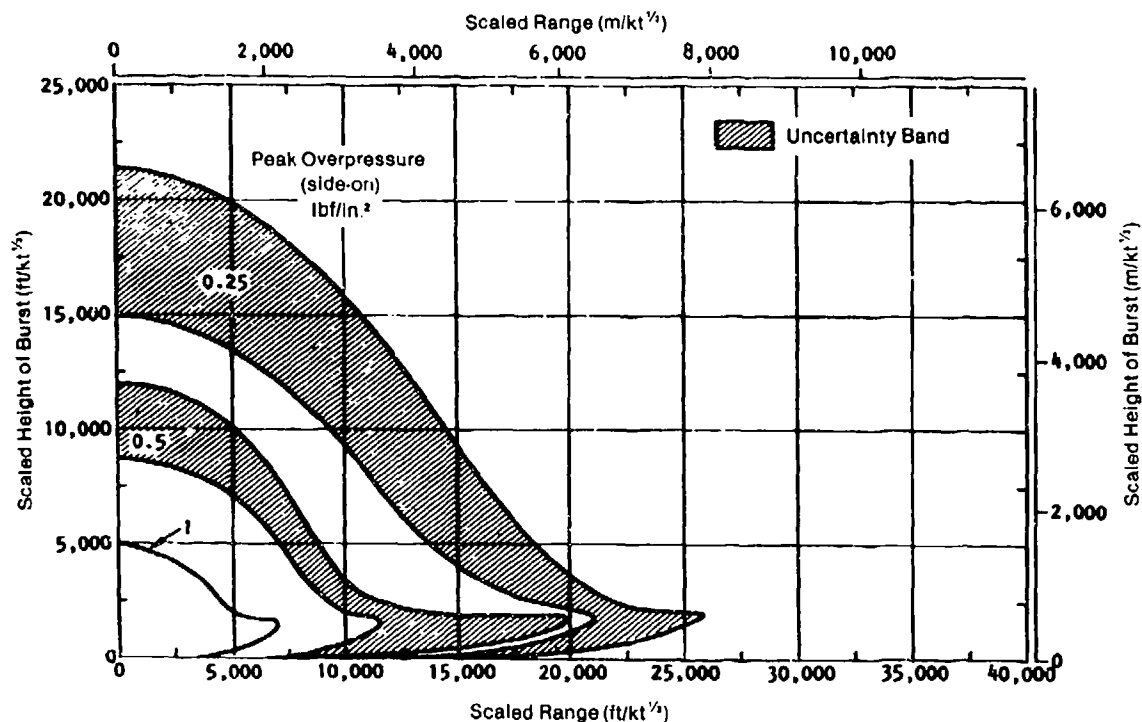
d. Very low overpressures in the far-field.

Figure 25 (cont'd).

Table 2. Thermal classification of ground surfaces (U.S. Army 1984).

Thermally near-ideal (precursor unlikely)	Thermally non-ideal (precursor may occur)
Water	Desert sand
Ground covered by white smoke layer	Coral
Heat-reflecting concrete	Asphalt
Frozen tundra	Surfaces with low, thick vegetation
Ice	Surfaces covered by a dark smoke layer
Packed snow	Dark-colored rock
[Moist] Soil with sparse vegetation	Most agricultural areas; residential areas in cities
Commercial and industrial areas	Dry soil with sparse vegetation

Attenuation curves for air blasts of nuclear origin are given in Figure 26. One curve shows the variation of peak overpressure with radius from ground zero for a contact burst. The other curve shows the variation of peak reflected overpressure with slant range. It gives the pressure at ground zero as a function of burst height, or the pressure as a function of slant range for points within a 30° cone under the burst point.

29
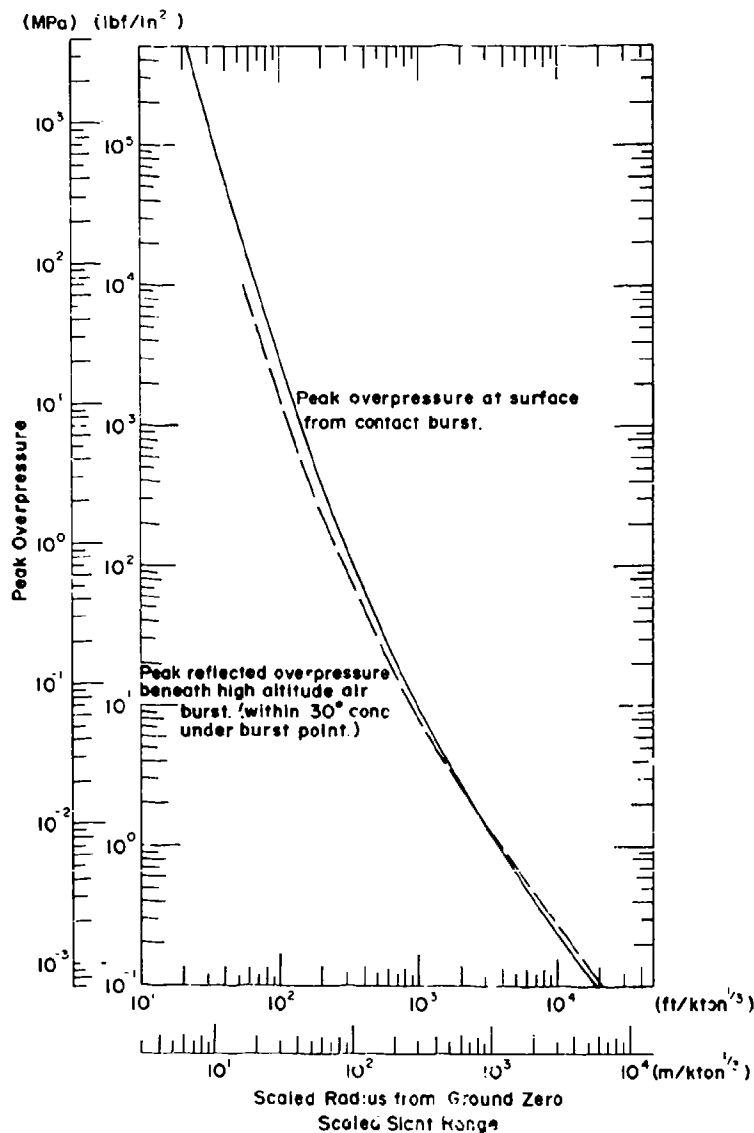
Figure 26. Attenuation curves for air blast
from nuclear explosions. The solid line gives
the variation of peak overpressure with ground-
level radius for a contact burst. The dashed
line gives the variation of peak reflected over-
pressure with slant range for an air burst (for
points within a 30° cone beneath the explosion).
Data from U.S. Army (1984) and DNA (1972).

Dynamic pressure represents a wind effect. It is zero at ground zero,
the center of radial symmetry; it increases with radius to a maximum and
then decreases with further increase of radius. Dynamic pressure is not
affected significantly by the thermal characteristics of the ground sur-
face, but it does vary with the amount of dust that is raised.

Figure 27. Variation of peak dynamic pressure with ground-level radius for a nuclear explosion over an ideal dust-free surface (U.S Army 1984, DNA 1972).

Figure 27 shows the variation of peak dynamic pressure with radius on an ideal surface which raises no dust. At close range the dynamic pressure is influenced by the height of burst, but beyond 350 ft/kt$^{1/3}$ (100 m/kt$^{1/3}$) there is not much dependence on height of burst. The close-range variation of peak dynamic pressure with charge height and radius is shown in Figure 28 for an ideal surface.

The effect of dust from loose surfaces is seen in the zone of Mach reflection (Fig. 29, 30). The effect is strongest for burst heights lower than 400 ft/kt$^{1/3}$ (120 m/kt$^{1/3}$), and at ranges closer than 1200 ft/kt$^{1/3}$ (370 m/kt$^{1/3}$). Between 400 and 1200 ft/kt$^{1/3}$ from ground zero, dust increases the peak dynamic pressure in comparison with dust-free conditions (Fig. 27, 28). At closer range, dust can lower the peak dynamic pressure.

The impulse for the positive phase is the integral of overpressure with respect to time, and so it is affected by the thermal properties of the ground surface. Figure 31 gives a representative distribution of im-
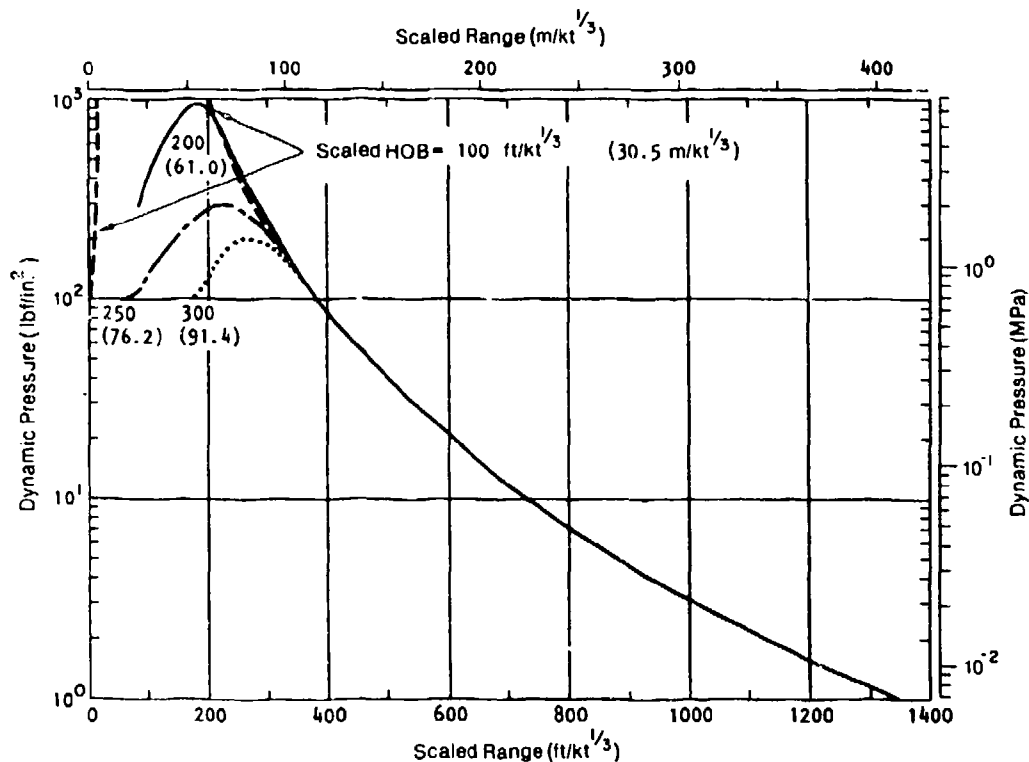
31
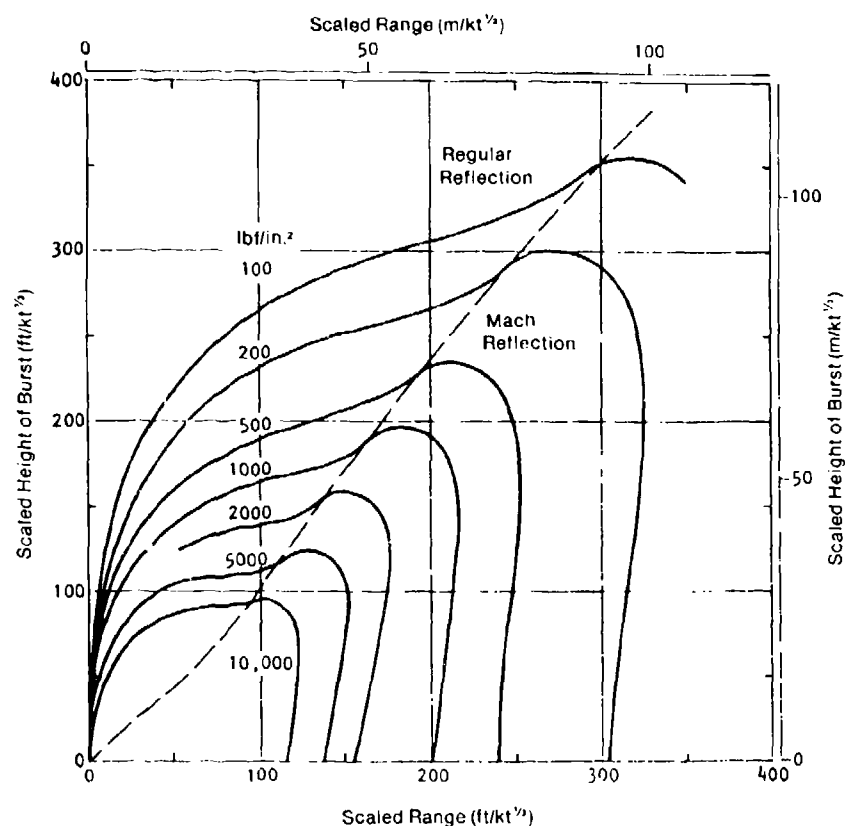
Figure 28. Variation of peak dynamic pressure with charge height and radius for a nuclear explosion over an ideal dust-free surface (U.S. Army 1984, DNA 1972).
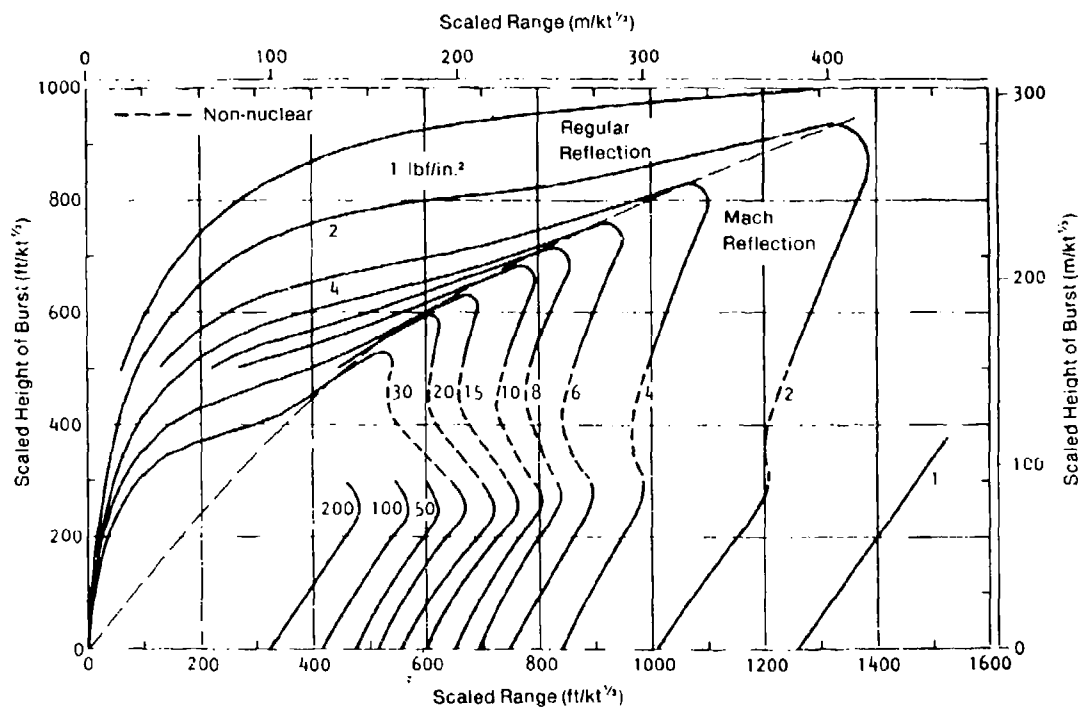
Figure 29. Variation of peak dynamic pressure with charge height and radius for a nuclear explosion over a surface where light dust conditions are generated (U.S. Army 1984, DNA 1972).
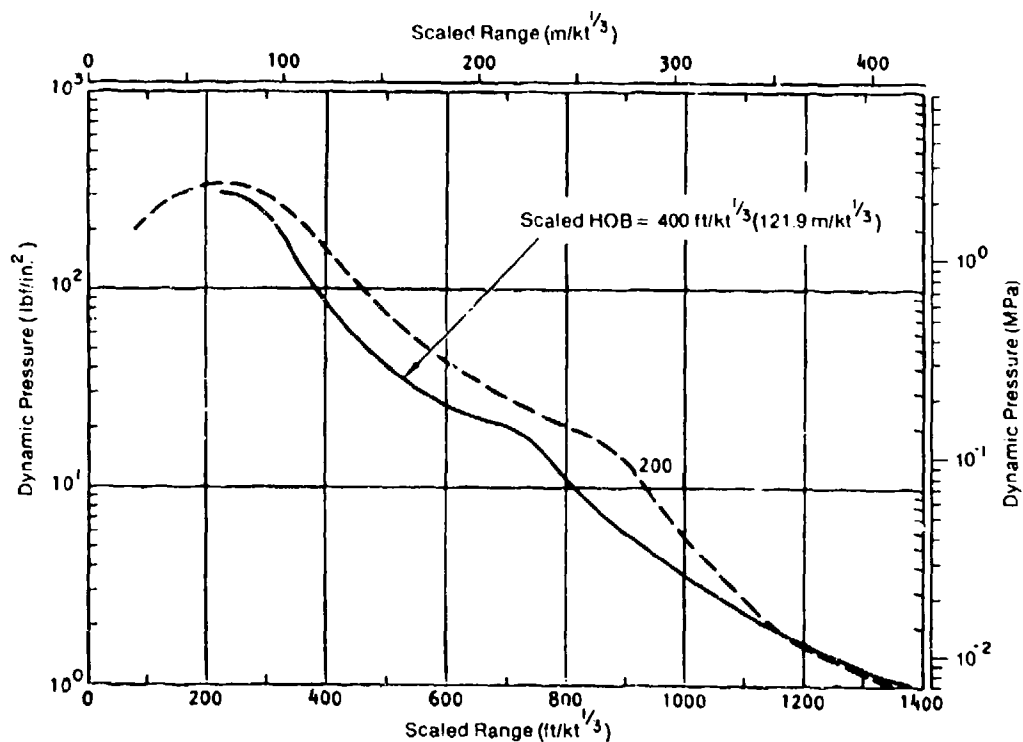
Figure 30. Variation of peak dynamic pressure with radius for nuclear air bursts over surfaces which generate heavy dust conditions. Adapted from U.S. Army (1984) and DNA (1972).
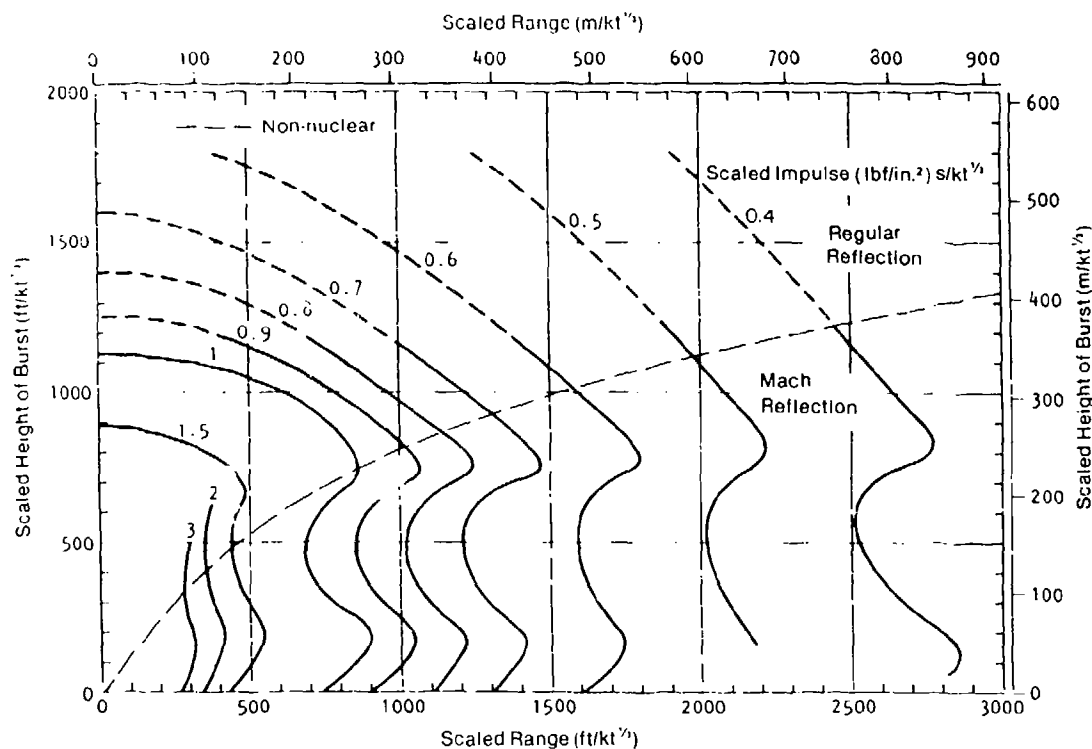
Figure 31. Variation of positive impulse with charge height and radius for nuclear explosions over a near-ideal surface (U.S. Army 1984, DNA 1972).
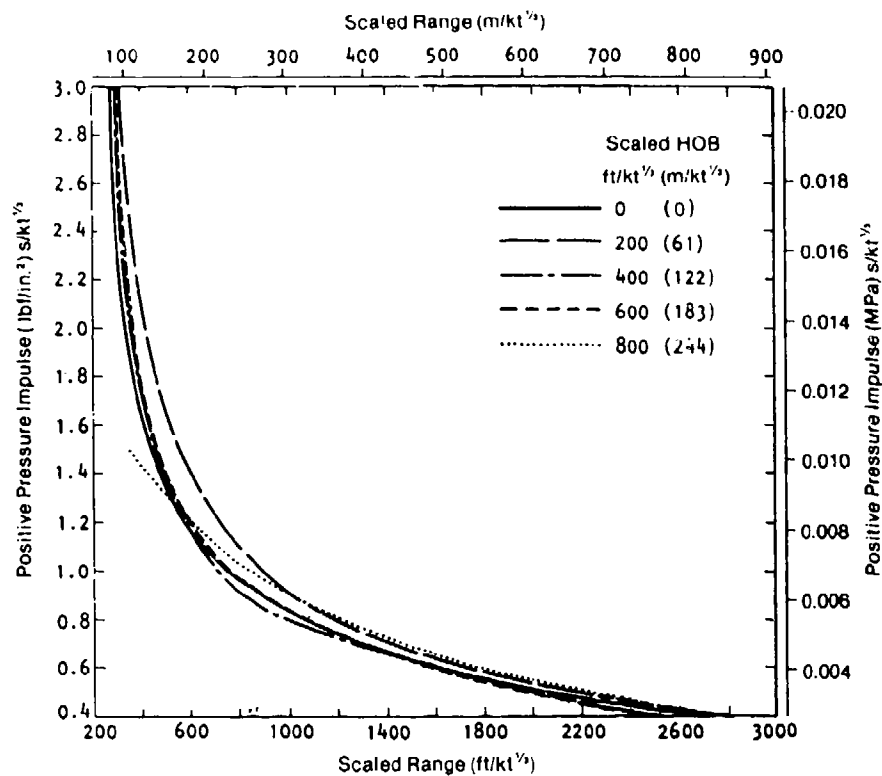
Figure 32. Attenuation curves for the positive impulse
from nuclear explosions over near-ideal surfaces (U.S.
Army 1984).
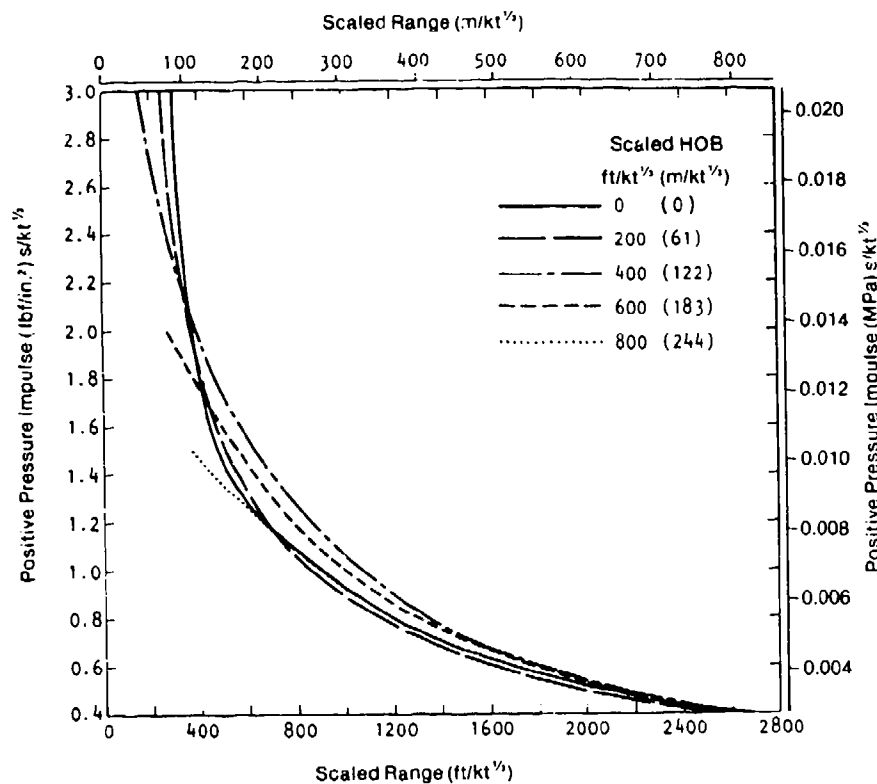
Figure 33. Attenuation curves for the positive impulse
from nuclear explosions over non-ideal surfaces (U.S.
Army 1984).

34
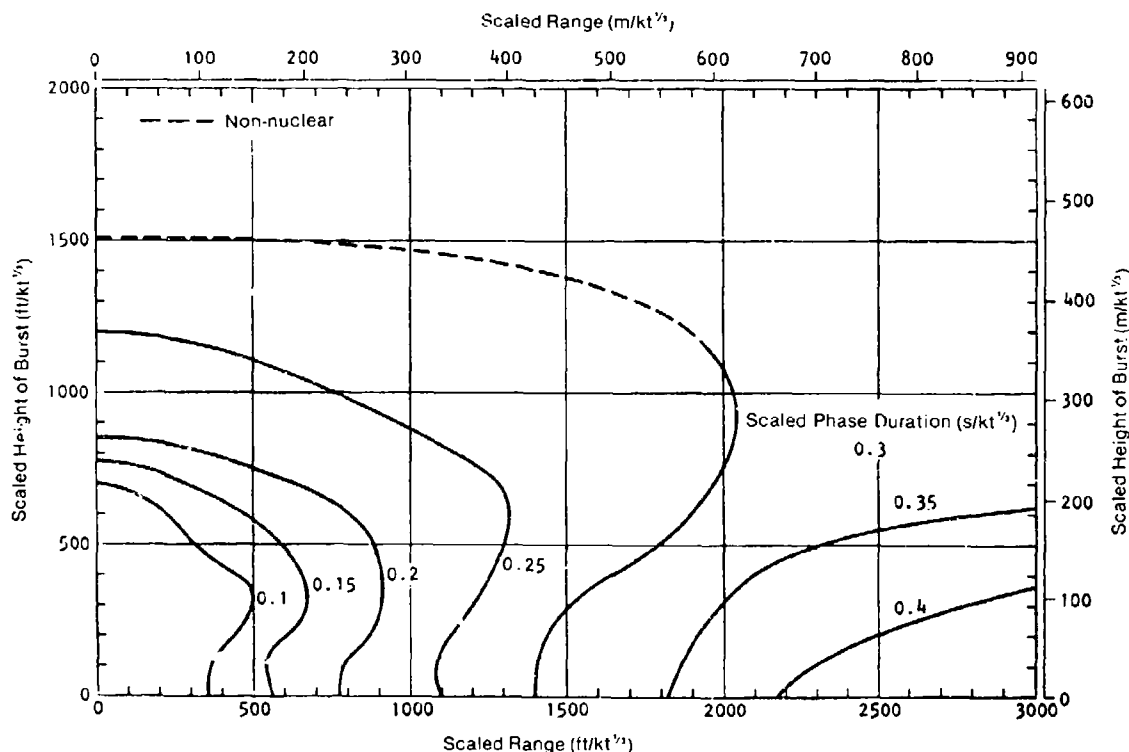
Figure 34. Variation of positive phase duration (overpressure) with charge height and radius for nuclear explosions over near-ideal surfaces (U.S. Army 1984, DNA 1972).

pulse for a surface that is near-ideal, and Figure 32 shows how the positive impulse at the surface attenuates. The distribution changes somewhat when the surface is non-ideal. Figure 33 shows how the attenuation curves for positive impulse at the surface are affected; in general, the impulse at close range tends to increase slightly by comparison with the near-ideal surface.

The distribution of phase duration for positive overpressures is shown in Figure 34 for a surface that has near-ideal thermal properties. When the surface is non-ideal, the distribution is distorted significantly, even for very high bursts and for large distances from ground zero (see U.S. Army Technical Manual 5-858-2 for details).

The phase duration for positive dynamic pressure is shown in Figure 35. This distribution is for surfaces where little or no dust is kicked up by the blast. When heavy dust is raised, phase duration changes significantly (see U.S. Army Technical Manual 5-858-2 for details).
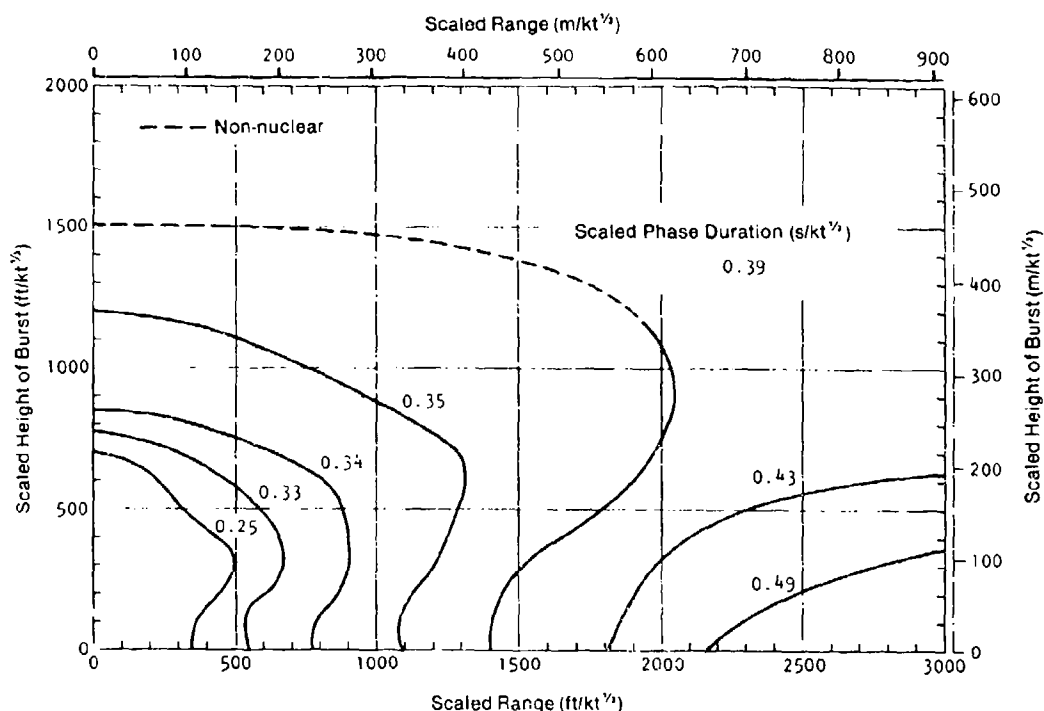
Figure 35. Variation of positive phase duration (dynamic pressure) with charge height and radius for nuclear explosions over surfaces where little or no dust is generated (U.S. Army 1984, DNA 1972).

The decay of pressure waves with time at a fixed location has been described mathematically by variants of the function xe^{-x}. Both overpressure and dynamic pressure have their maximum values at the shock front and, for a given location, both decrease to zero at about the same time (the positive phase of the dynamic pressure is actually slightly longer than that of the overpressure). Except in regions of very high overpressure ($p_m > 70$ lbf/in.^{2}, or > 0.5 MPa), peak dynamic pressure is less than peak overpressure, and their rates of decay are therefore different. The exponential decay of overpressure and dynamic pressure at a given point has been described by the empirical relations

$$\frac{p}{p_m} = \left(1 - \frac{t}{t_+}\right) \exp \left(- \right) \tag{25}$$

$$\frac{q}{q_m} = \left(1 - \frac{t}{t_+}\right)^2 \exp \left(-\frac{2t}{t_+}\right) \tag{26}$$

where p and q are the transient overpressure and dynamic pressure at time t, and t_+ is the positive phase duration (Glasstone 1962). Figures 36 and

36
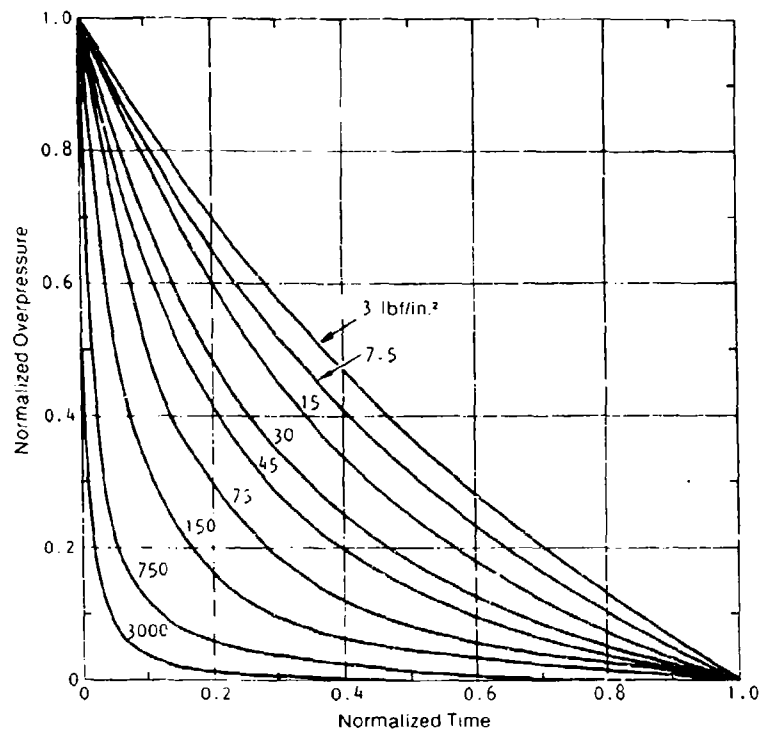
a. Curves from U.S. Army (1984) and DNA (1972).
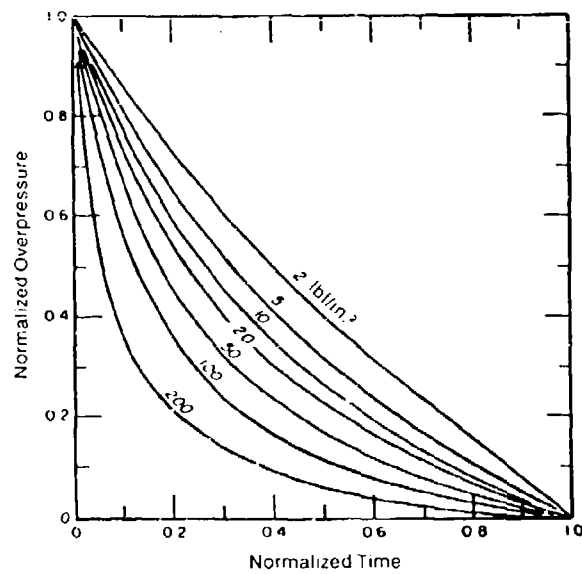
b. Curves from Glasstone (1962).

Figure 36. Idealized exponential decay of positive overpressure with time at sea level. See text for normalizing parameters.

37
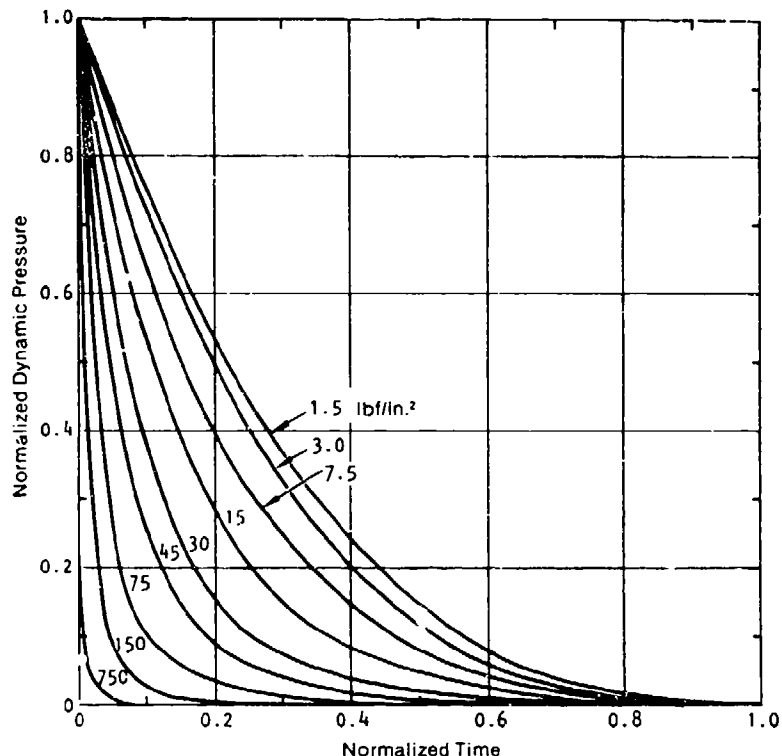
a. Curves from U.S. Army (1984) and DNA (1972).
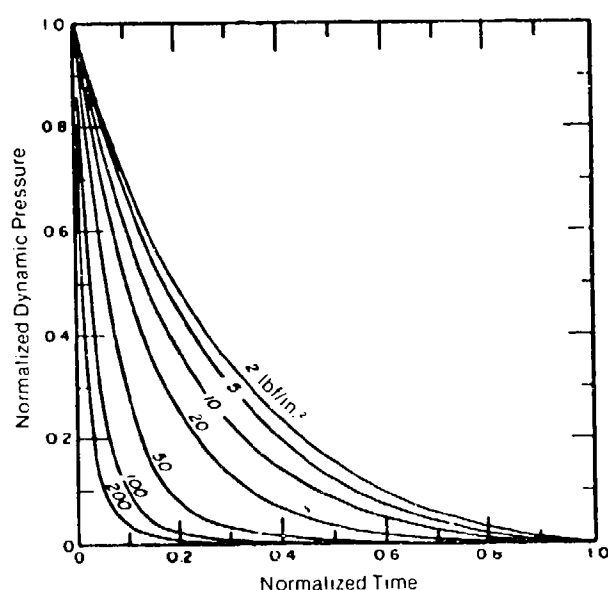
b. Curves from Glasstone (1962).

Figure 37. Idealized exponential decay of positive
dynamic pressure with time at sea level. See text
for normalizing parameters.

38

37 give some accepted approximations of the wave decay for overpressure and dynamic pressure.

Air Blast from Underground Explosions

Air blast is muffled when the charge is detonated below the ground surface. In general, there are two identifiable pulses in the air blast record from an underground explosion. The first is identified with ground shock, i.e. there is an initial transfer of energy to the air when the shock wave hits the ground/air interface. The second is induced by ground motion and venting as the gas bubble bursts through the surface. In hard ground that can transmit shock without much dissipation, the first pulse, induced by ground shock, may be dominant. In soft ground that absorbs shock, the second pulse, induced by venting, may be the dominant one.

Estimates of air blast from buried charges are based on the data for surface charges (Fig. 20, 26). An air blast prediction is made for a surface explosion, with appropriate adjustments for ambient environmental conditions. Thereafter, the predicted overpressure can be obtained either by applying a damping factor to the surface-burst pressure, or by applying a multiplying factor to the range scale of the curve for surface bursts.

In the method given by Johnson (1971), the predicted peak overpressure for a surface burst is multiplied by a damping factor (Fig. 38), and the result is the peak overpressure for the dominant pulse of the underground explosion, without regard for whether the ground shock pulse or the venting pulse is the dominant one. The damping factor is a function only of charge
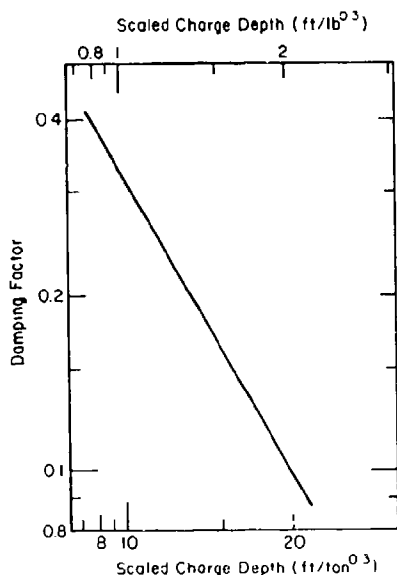
Figure 38. Air blast damping factor as a function of charge depth for large buried explosions. The air blast overpressure for a surface charge is multiplied by the appropriate damping factor to predict the air blast overpressure for a buried explosion. After Johnson's (1971) adaptation of a relation by Reed.

39
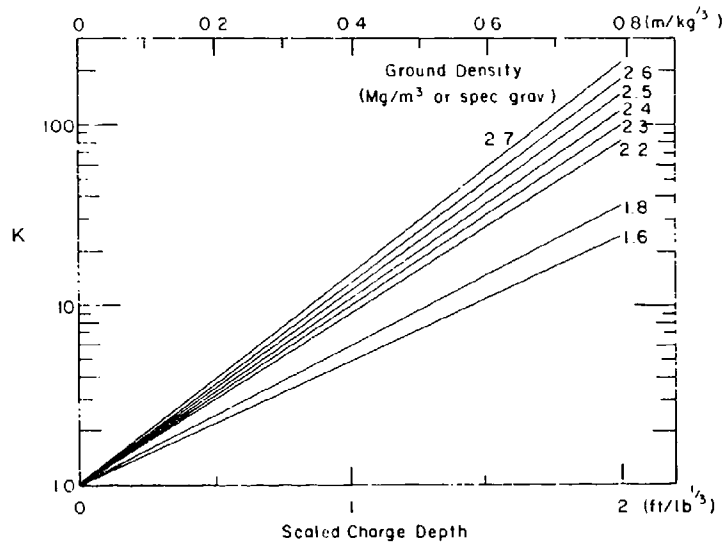
Figure 39. Range multiplication factor K for
predicting air blast from buried explosions.
To obtain the overpressure p at a specified
scaled range $\bar{r}$ from the underground explosion,
read from Figure 16 (or equivalent curve) the
value of p at scaled radius K$\bar{r}$. Graphical
version of computational procedure given by
Swisdak (1975).

depth, without reference to ground material. In the method described by
Swisdak (1975), the range is adjusted by a multiplying factor, such that
the range for a given overpressure becomes greater for a buried explosion
than for a surface explosion. The multiplication factor, which is a func-
tion of charge depth and ground density, is obtained by raising e to a di-
mensional power. This technical impropriety could be remedied by convert-
ing scaled charge depth in $ft/lb^{1/3}$ to a dimensionless value from Figure
5, but for present purposes it is easier to give the multiplier K in graph-
ical form (Fig. 39). To predict the overpressure p at a specified range r
for a given underground explosion (weight W), an appropriate value of K is
obtained from Figure 39, r is scaled as $r/W^{1/3}$, and p is read from a sur-
face burst curve (Fig. 20) for a distance of K $r/W^{1/3}$.

When a row of cratering charges is fired simultaneously the peak over-
pressure at a distance is usually reinforced. Figure 40 gives multiplica-

40

Figure 40. Overpressure multiplier
for air blast from a row charge. If
the point of concern is in line with
row of charges, use the lower line.
If the point of concern is off to
one side of the row, and reasonably
distant, use the upper line. From
Johnson (1971).

tion factors for row charges. This is based on observations for row
charges at practical spacings. In principle, there are charge spacings and
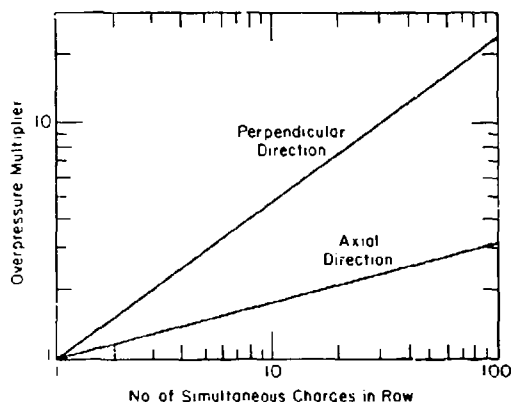range positions which do not necessarily give amplification; waves from the
individual charges can interfere in a variety of ways, including superposi-
tion of positive and negative phases.

In normal blasting operations, air blast is not the controlling damage
criterion; ground motion is likely to become a problem before air blast
causes damage.

Air Blast from Underwater Explosions

Detonation underwater greatly reduces airblast in comparison with sur-
face detonation, even at very shallow scaled depth. Figure 41 gives con-
tours of peak overpressure, showing how air blast varies with charge depth
and with horizontal distance from "surface zero," the point directly above
the charge. Contours are given for horizontal planes at three different
heights above the water surface. Point values of peak overpressure for a
surface burst over solid ground are also shown on the graph*. Data for
greater scaled heights are given by Swisdak (1978).

---

* Attenuation curves given by Hallanger (1976) for air blast overpressure
from underwater explosions seem questionable. The indicated air blast from
some shallow underwater explosions is greater than air blast from surface
bursts, and the indicated attenuation is acoustic (n = -1) for all levels
of overpressure.

41
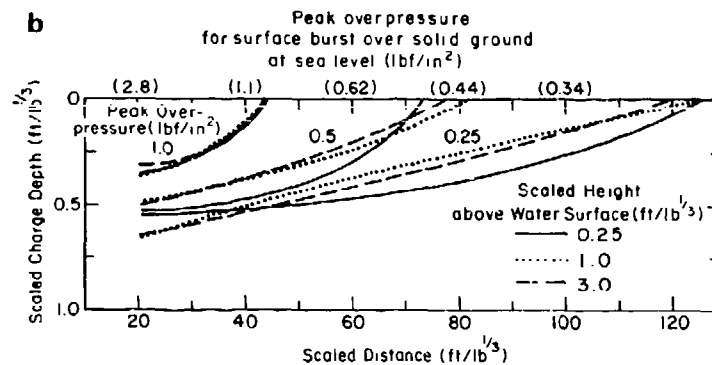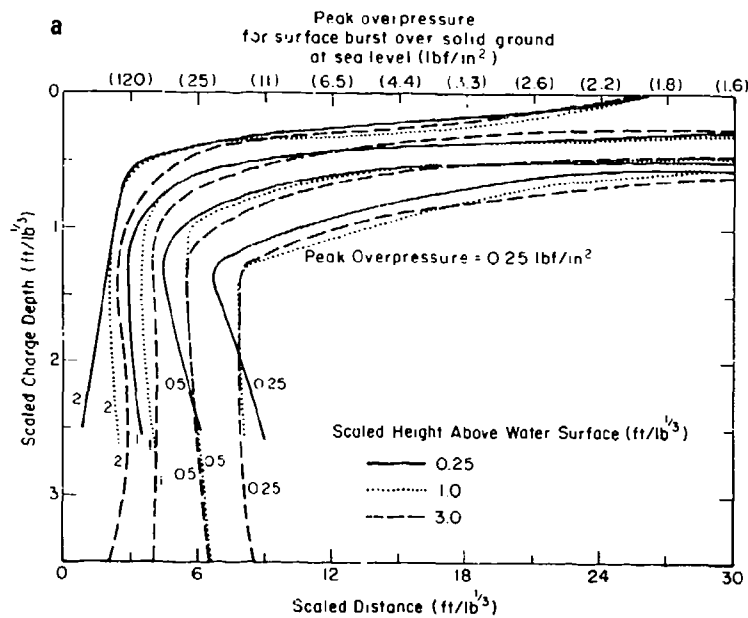
Figure 41. Air blast overpressure from under-
water explosions. The plot shows the effect of
charge depth, radius from surface zero, and the
height of observation above water level. Fig-
ure 41a shows the general pattern, while Figure
41b gives more detail for fairly long ranges.
Intersections of the contours with the axis for
zero charge depth give the attenuation for a
surface burst over water. The figures in par-
entheses are the surface-level overpressure
values that occur at the indicated distances
for a surface burst over solid ground. Adapt-
ed from Swisdak (1975).

Air Blast Damage Criteria

Structural damage from air blast depends on the characteristics cf the air shock, principally peak overpressure and phase duration, and also on the characteristics of the structural element, mainly frequency response and strength. In cases of severe damage where dynamic pressure is a factor, the drag characteristics and "porosity" of the target may also be important.

Damage criteria are based on peak overpressure, making the tacit assumption that phase duration does not vary significantly for a given overpressure. Such an assumption seems justifiable for limited ranges of explosive yield, since phase duration follows cube root scaling, but significantly different waveforms are possible (e.g. the long-period N-wave of a sonic boom). Approximate overpressure levels for positive damage are shown in Figure 42, together ith the safe limit accepted by the U.S. Bureau of Mines.

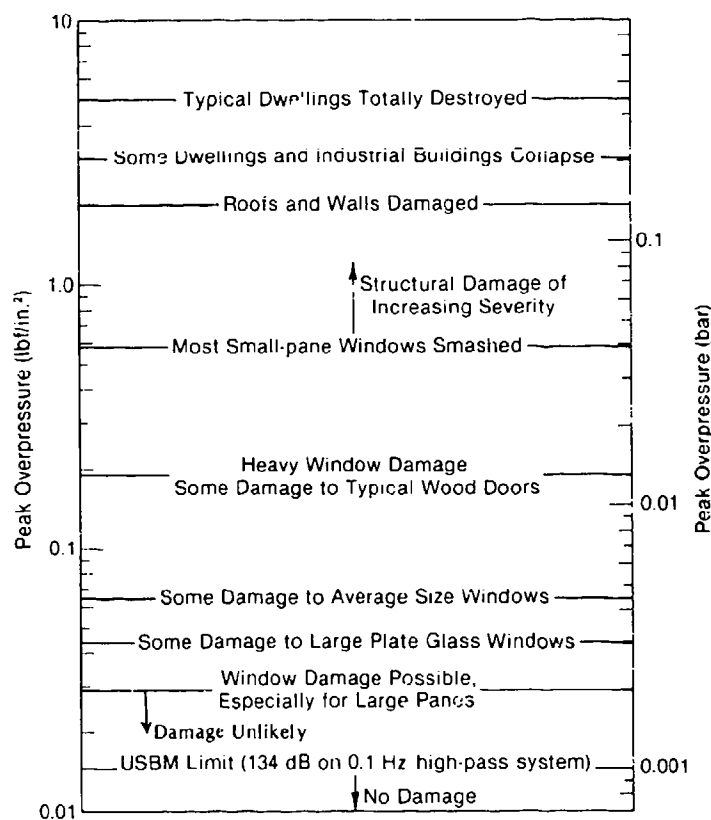Figure 42. Approximate values of overpressure at which various kinds of damage are likely to occur. Data from various sources, e.g. Glasstone (1962), Siskind et al. (1980), du Pont (1977).

43

In civil blasting operations the emphasis is on limiting air blast to safe or tolerable levels, and on verifying the limits. Air blast at these levels is commonly perceived as noise of relatively high frequency rather than as shock, and safe limits are usually expressed in decibels (dB). Measured values depend to some extent on the response characteristics of the sensor, and safe limits are specified with reference to the measuring device. Table 3 gives the USBM safe limit for various types of measuring systems.

Table 3. USBM safe limits for air blast.

Characteristic of measuring system	Safe limit dB	$lbf/in.^2$
0.1 Hz high-pass	134	0.0145
2 Hz high-pass	133	0.013
5 Hz or 6 Hz high-pass	129	0.0082
C-slow (events not exceeding 2 s duration)	105	0.00052

Air blast intensity in decibels I is related to the pressure level p by

$$I = 20 \log_{10} (p/p_*) \quad dB \qquad (27)$$

where p_* is a reference level of air pressure taken as 2×10^{-4} dyne/cm^2 (2.9×10^{-9} $lbf/in.^2$) at 20°C.

Effects of Ambient Pressure and Temperature

The effects of an explosion in free air are much the same in cold regions as they are anywhere else, although the temperature and pressure of the ambient air can produce some minor quantitative differences. Cold regions tend to have lower air temperatures and some regions, notably Greenland and Antartica, have high surface elevations, with consequent low values of atmospheric pressure and density. Figures 43 and 44 show how pressure, temperature, density and acoustic velocity vary with altitude in free air.

In a homogeneous air mass, the peak air blast overpressure p_m at a given scaled radius varies with the ambient air pressure p_0 such that the shock strength is constant for constant scaled radius. Since the shock strength is the ratio of absolute pressure behind the shock front to the ambient pressure, i.e. $(p_m+p_0)/p_0$, we can write:

44

$$\frac{P_{m1}}{P_{01}} + 1 = \frac{P_{m2}}{P_{02}} + 1 \qquad (28)$$

where subscripts 1 and 2 denote two different levels of ambient pressure (or altitude), and the scaled radius is constant. Thus, at a given scaled distance from an explosion, the peak overpressure will vary directly with the atmospheric pressure as

$$\frac{P_{m2}}{P_{m1}} = \frac{P_{02}}{P_{01}} . \qquad (29)$$

In other words, if P_{m1} is the peak overpressure given by standard curves adjusted to sea level pressure (1 atmosphere, or 14.7 lbf/in.^{2}), that figure has to be adjusted by a factor (P_{02}/P_{01}) to obtain the peak overpressure at the same scaled radius when the atmospheric pressure is P_{02}.
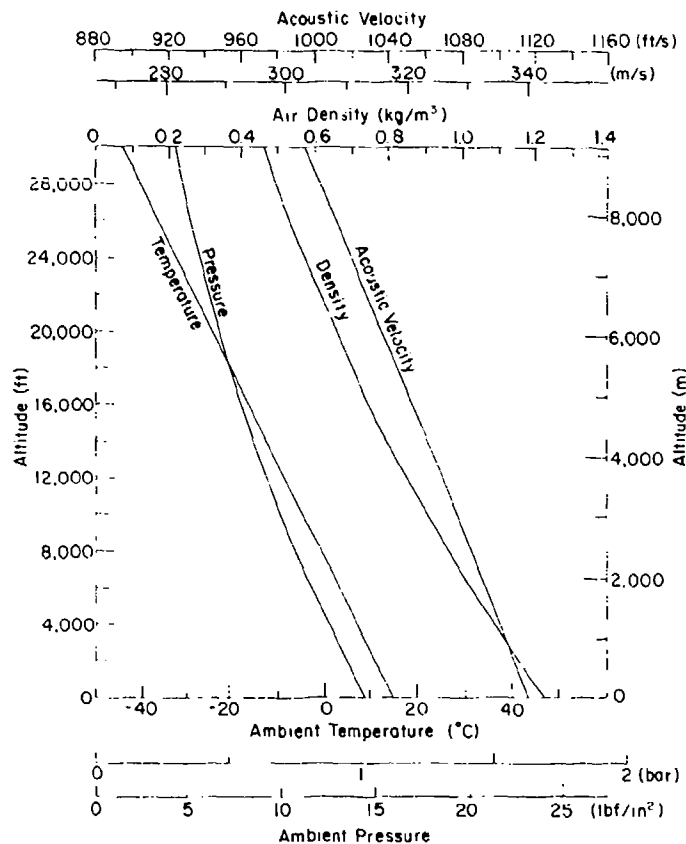

Figure 43. Variation of atmospheric properties with altitude according to U.S. Standard Atmosphere of 1962.
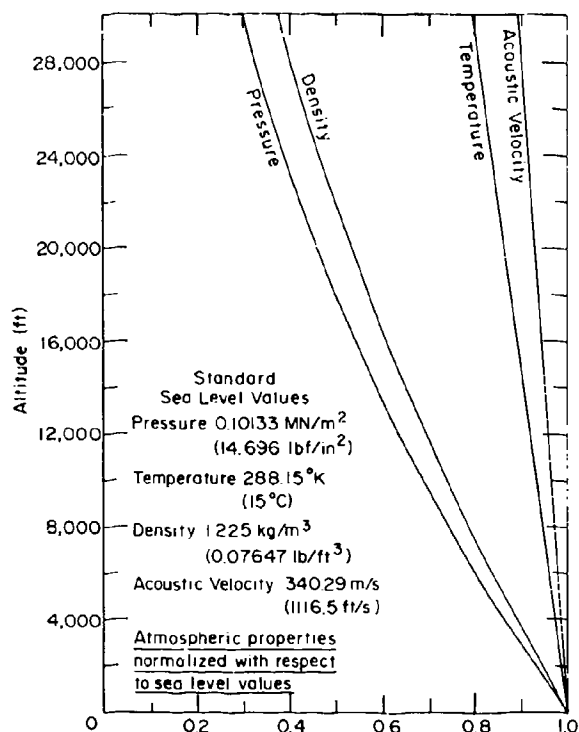
45

Figure 44. Relative values of atmospheric properties as functions of altitude, according to U.S. Standard Atmosphere of 1962.

The effect of atmospheric pressure on the scaled radius $\bar{r}$ for a fixed value of p_m/p_o is given by Sachs scaling as:

$$\frac{\bar{r}_2}{\bar{r}_1} = \left(\frac{p_{02}}{p_{01}}\right)^{1/3} \tag{30}$$

where $\bar{r}_1$ and $\bar{r}_2$ are the scaled radii where a fixed value of p_m/p_o is experienced with ambient pressure levels p_{01} and p_{02}.

The net effect produced by a change of atmospheric pressure is estimated from a two-step procedure. The scaled radius is adjusted in accordance with eq 30, and the peak overpressure for that adjusted scaled radius at the reference elevation is multiplied by the factor given by eq 29. Figures 15-18 indicate how ambient pressure influences the standard blast parameters.

Ambient air temperature affects density, wave velocity, arrival time and phase duration. Combining the effects of atmospheric pressure and ambient air temperature, the initial density varies as

$$\frac{\rho_{02}}{\rho_{01}} = \frac{p_{02}}{p_{01}} \cdot \frac{T_1}{T_2} \tag{31}$$

46

Sonic velocity in the ambient air varies as

$$\frac{c_{02}}{c_{01}} = (\frac{T_2}{T_1})^{1/2} \qquad (32)$$

and shock velocity varies in the same way. The arrival time t_2 at the adjusted radius $\bar{r}_2$ given by eq 30 is

$$\frac{t_2}{t_1} = (\frac{p_1}{p_2})^{1/3} (\frac{T_1}{T_2})^{1/2} \qquad (33)$$

and positive phase duration varies in the same way. The impulse, which is the integral of overpressure with respect to time, is adjusted by a factor made up from the adjustment factors for overpressure and time, i.e.

$$\frac{I_2}{I_1} = (\frac{p_{02}}{p_{01}})^{2/3} (\frac{T_1}{T_2})^{1/2} \quad . \qquad (34)$$

Convenient tables and graphs for adjusting blast parameters in accordance with Sachs scaling are given by Swisdak (1975).

Explosions in Vacuum or in Space

Having noted that the standard altitude adjustments are not valid for very big differences of altitude, it is worth considering briefly the limiting condition when pressure tends to zero. In a vacuum, or in space, the ambient pressure and density are effectively zero. If the explosion source functions normally, it generates explosion products at high initial pressure and temperature, but it cannot impart mechanical disturbance to the surround'ngs because there is nothing there. Since the explosion products, in the form of particles and gas molecules, receive momentum from the explosion process, they ought to travel outward indefinitely without resistance, but subject to gravity. If the explosion source produces radiation, as a nuclear source does, the radiation will be transmitted, subject only to geometrical attenuation.

Air Blast Attenuation Over Snow Surfaces

Air blast measurements have been made for propagation over the surface of deep snow, and some results are given in Figure 45. Since all these measurements were made at high altitude, the data are adjusted to a common surface elevation of 6000 ft (1830 m). For comparison with standard sea level data, the curve of Figure 45 has to be shifted up in accordance with the adjustment procedures described earlier. At overpressures above 1
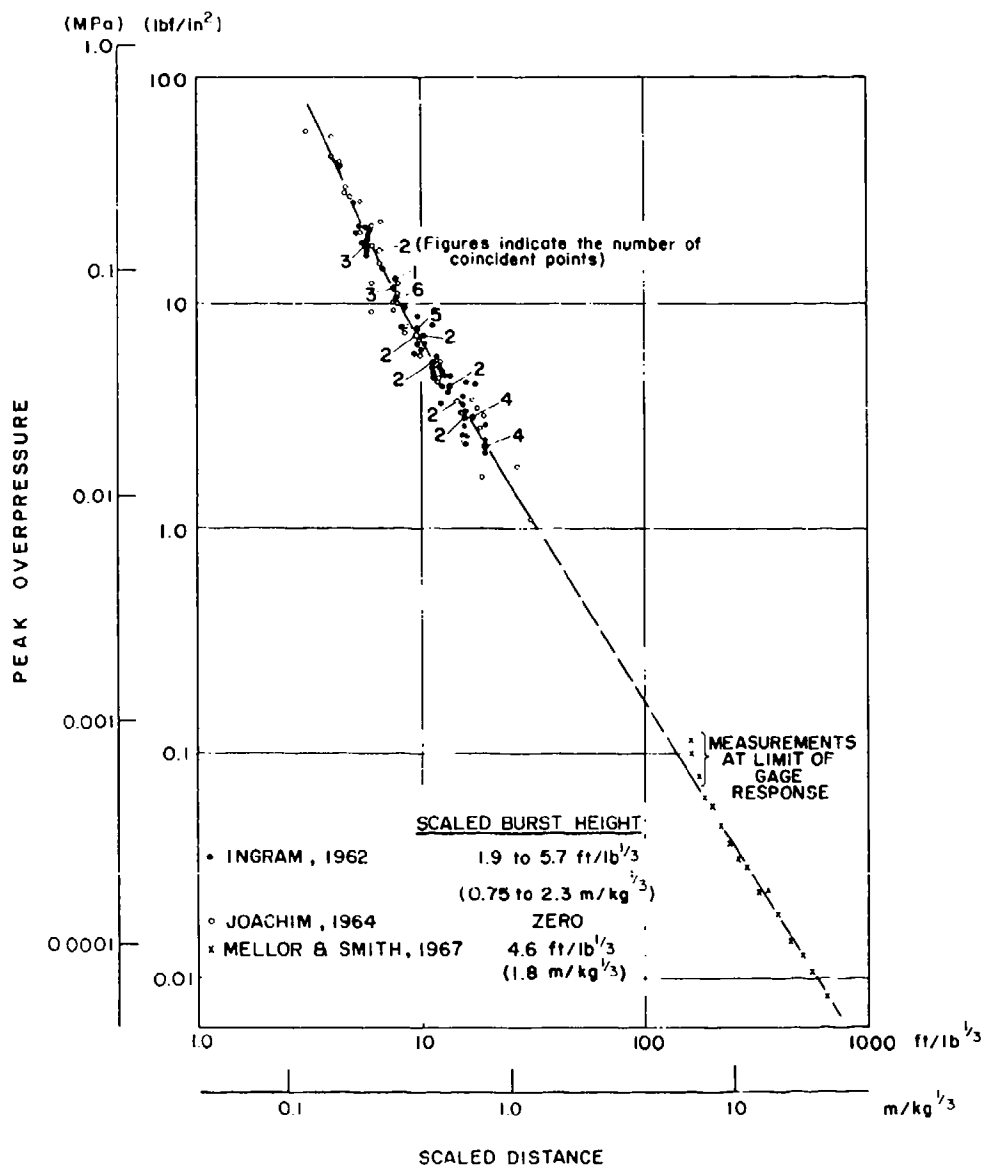
47

Figure 45. Air blast attenuation over the surface of very deep snow. All measurements were made at high altitude and the data have been adjusted to a common surface elevation of 6000 ft (1830 m).

lbf/in.^{2} (7 kPa) there is close agreement, but the far-field measurements over snow are lower than the values predicted by <u>extrapolation</u> of the standard curves. The rate of attenuation for the far field is such that overpressure is approximately proportional to $r^{-1.6}$.

Measurements of overpressure and positive-phase impulse were also made over seasonal snow cover (Wisotski and Snyer 1966), using small charges (1 lb, or 0.45 kg) and scaled thicknesses for the snow cover in the range 0.23

48

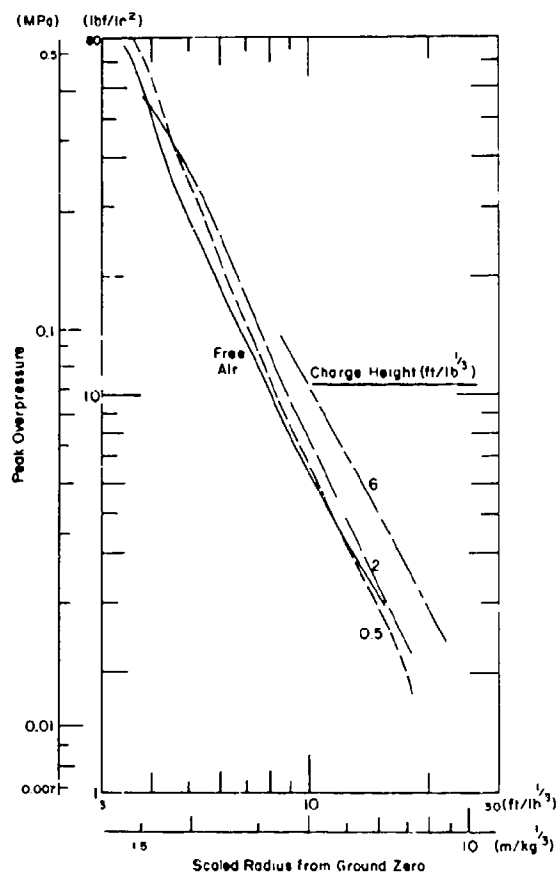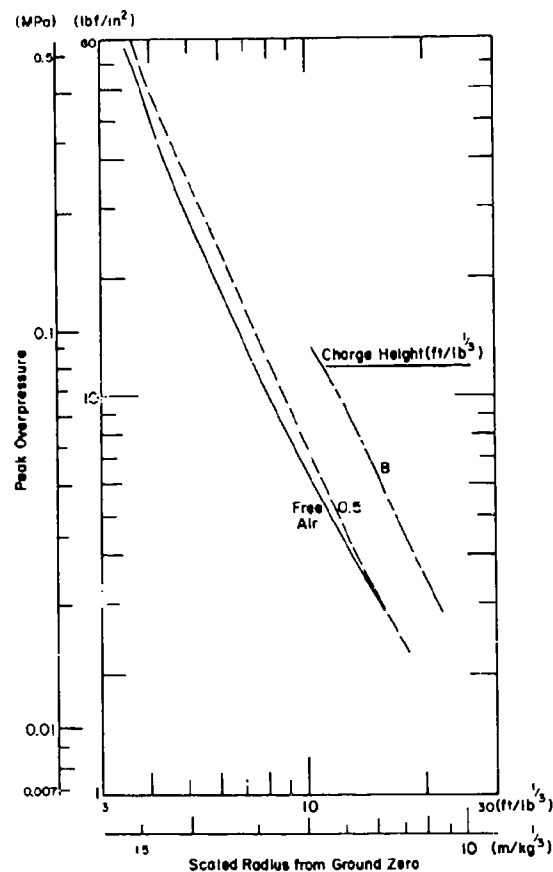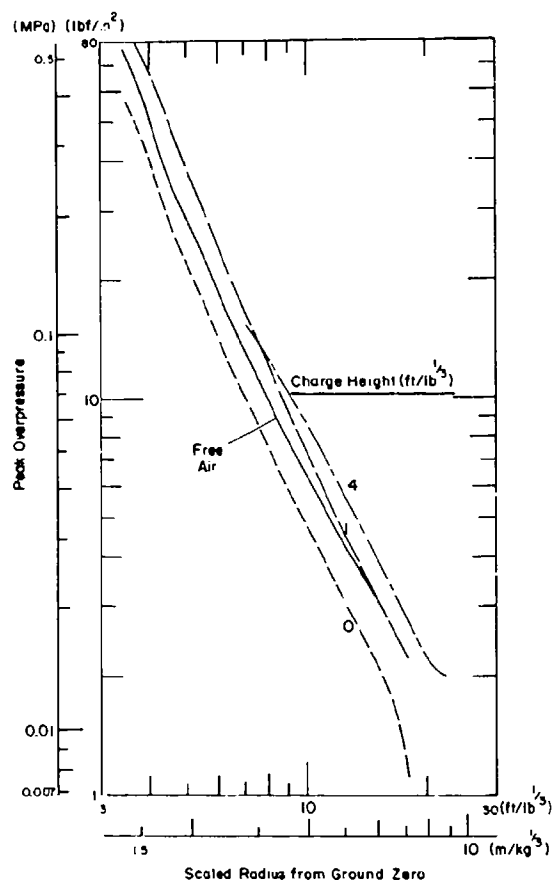Figure 46. Air blast attenuation over seasonal snow (scaled thickness 0.23 to 1.65 m/kg$^{1/3}$, or 0.58 to 4.2 ft/lb$^{1/3}$). These measurements were made at an altitude of 10,800 ft (3292 m). Summary of results by Wisotski and Snyer (1966).
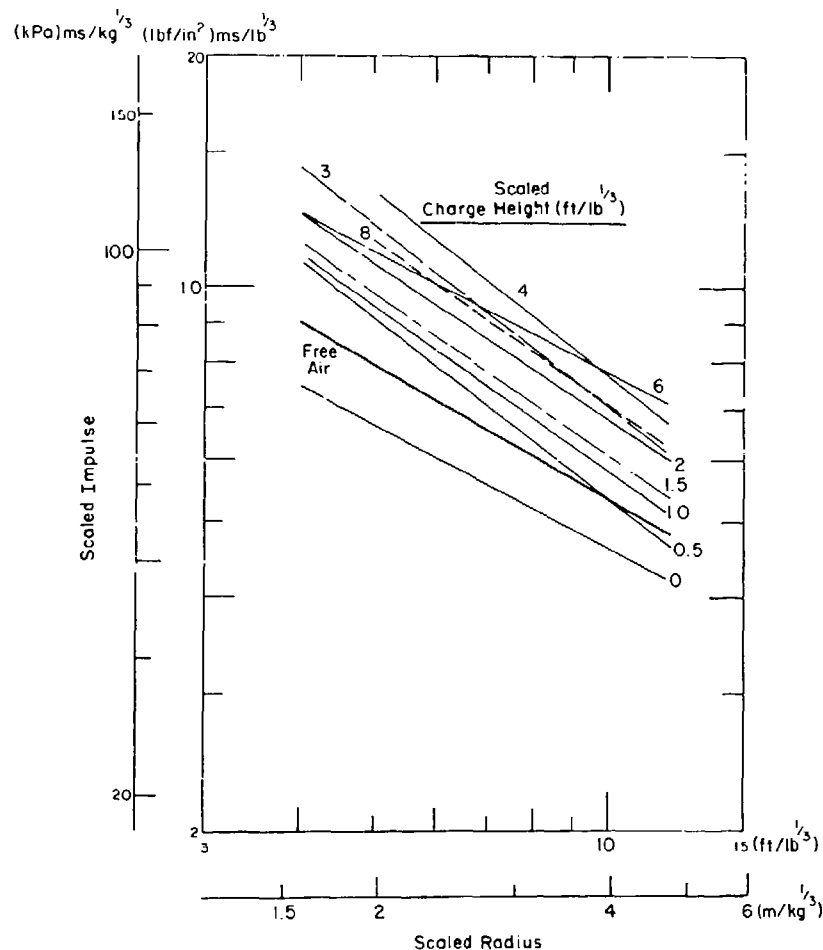
49

Figure 47. Attenuation of positive impulse over sea-
sonal snow (thickness and site altitude as for Fig.
46). Summary of results by Wisotski and Snyer (1966).

to 1.65 m/kg$^{1/3}$ (0.58 to 4.2 ft/lb$^{1/3}$). The altitude of the site was
3292 m (10,800 ft), with average ambient pressure 0.68 bar. The oversnow
attenuation curves for overpressure, with charge height as parameter, are
shown in Figure 46. For the range of the data, overpressure is approxi-
mately proportional to $1/r^2$.

The corresponding impulse data of Wisotski and Snyer show considerable
scatter; the trend lines are given in Figure 47. Impulse is roughly pro-
portional to $r^{-0.7}$ for this range.

Shock Reflection from Snow Surfaces

Simple theory for shock reflection assumes a rigid reflecting surface,
so that no energy is lost in the reflection process. However, when the re-
flecting surface can absorb energy by inelastic deformation, the amplitude
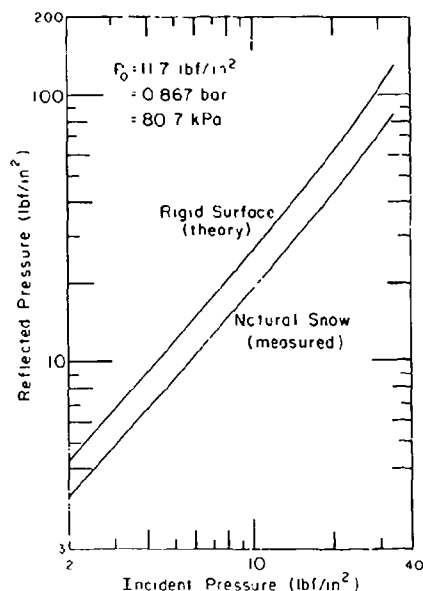
50

Figure 48. Reflected pressure as a function of incident pressure for relatively strong air blast over deep ice cap snow (measured) and over a rigid surface (theoretical). After Ingram (1962).
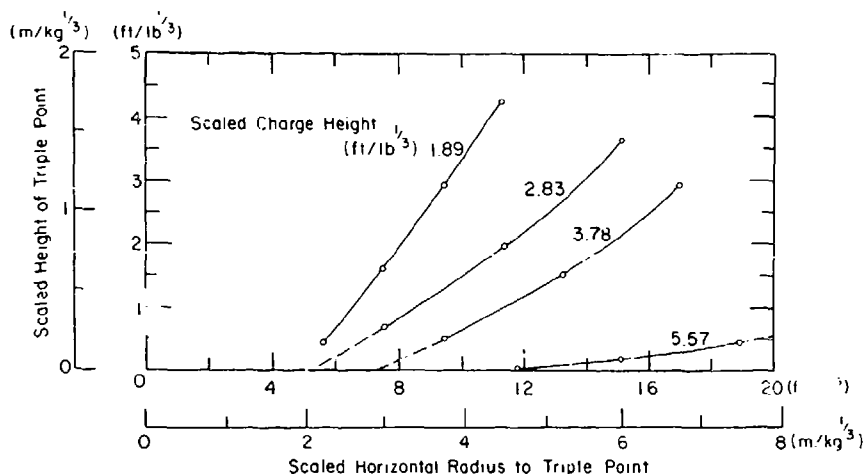
Figure 49. Height of the triple point (Mach stem) as a function of radius and charge height for shock reflection over deep, dense snow at high altitude. From Ingram (1962).

of the reflected wave ought to be less than that for reflection from a rigid surface.

Figure 48 summarizes the results of measurements made on the Greenland ice cap, where air blast from high explosive charges was reflected from the surface of dense, but very deep, snow. The reflected pressure was significantly lower than the theoretical reflected pressure over a rigid surface, as calculated from eq 23.

Figure 49 gives some data for the height of the triple point (height of Mach stem) for shock reflection over deep snow at high altitude. Com-

51

paring these curves with the "standard" curves of Figure 8, it can be seen that the snow surface curves are displaced downward. In other words, the locus of the triple point is closer to the surface than might be expected.

Wisotski and Snyer (1966) made measurements over seasonal snow cover (thickness 0.23 to 1.65 $m/kg^{1/3}$) and also over bare ground. Their measurements of peak overpressure p_m for the region of Mach reflection show that p_m is higher over bare ground than over snow for given values of radius and charge height (Fig. 50). The general pattern of behavior is also illustrated in Figure 51.
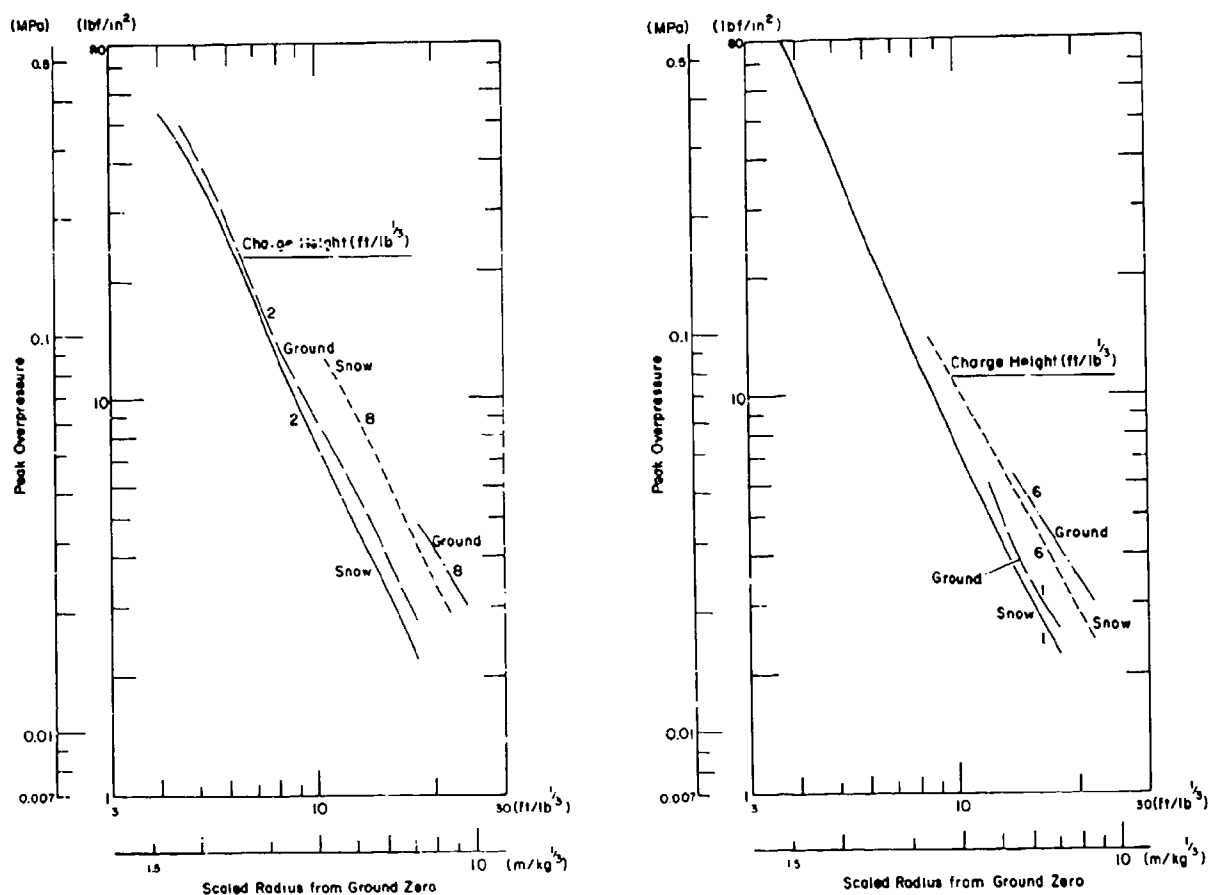
Figure 50. Peak reflected overpressure (Mach region) as a function of radius and charge height, comparing measurements over seasonal snow and measurements over bare ground (see Fig. 46 for site conditions). Summary of results by Wisotski and Snyer (1966).

52

Figure 50 (cont'd).

Figure 51. Variation of peak overpressure with radius and charge height for explosions over seasonal snow cover and over bare ground at high altitude. From Wisotski and Snyer (1966).
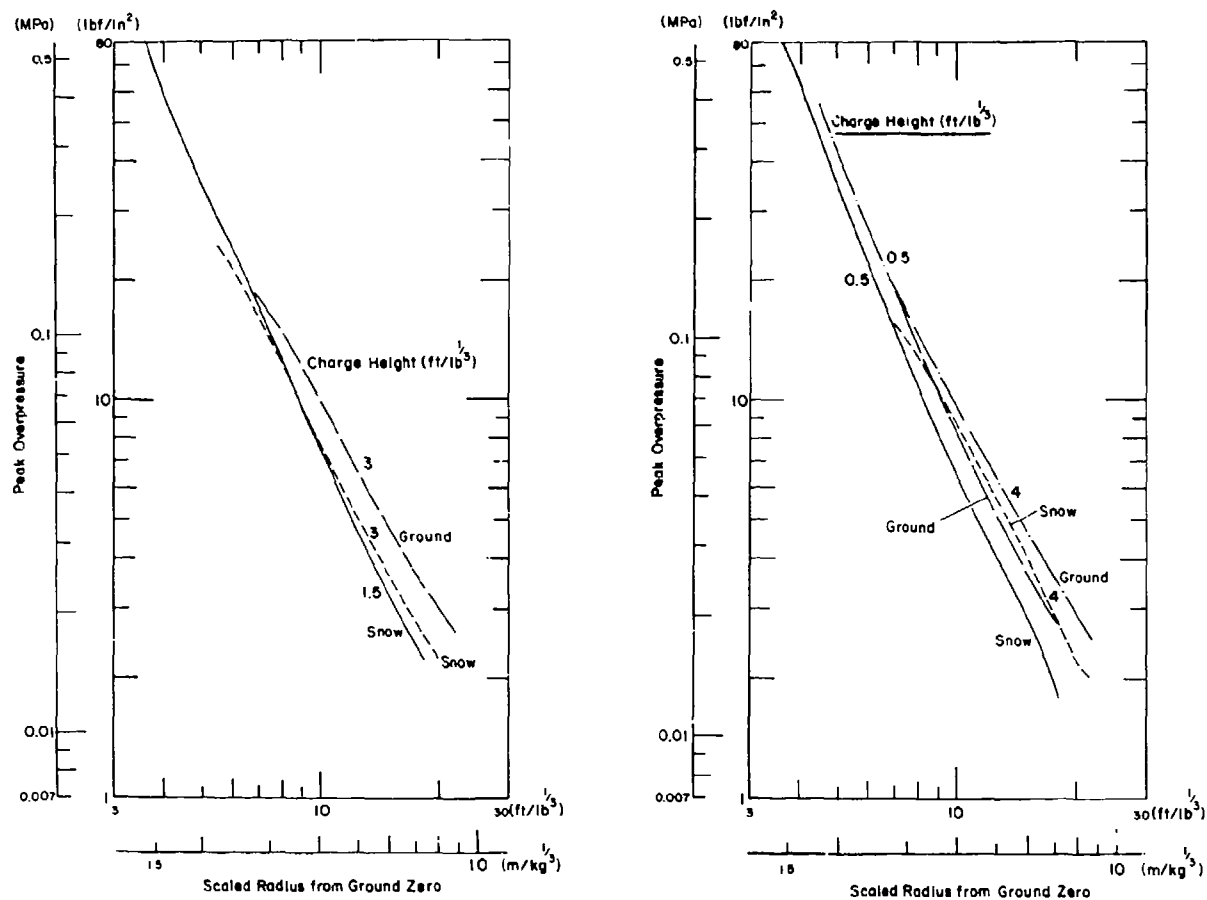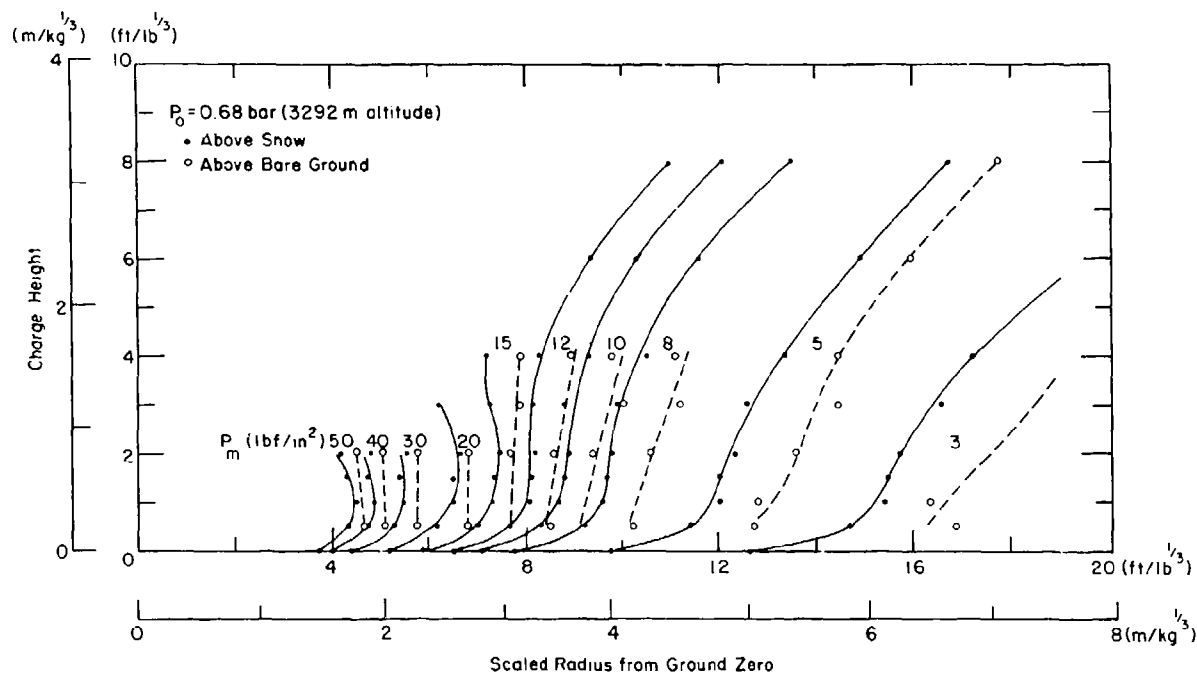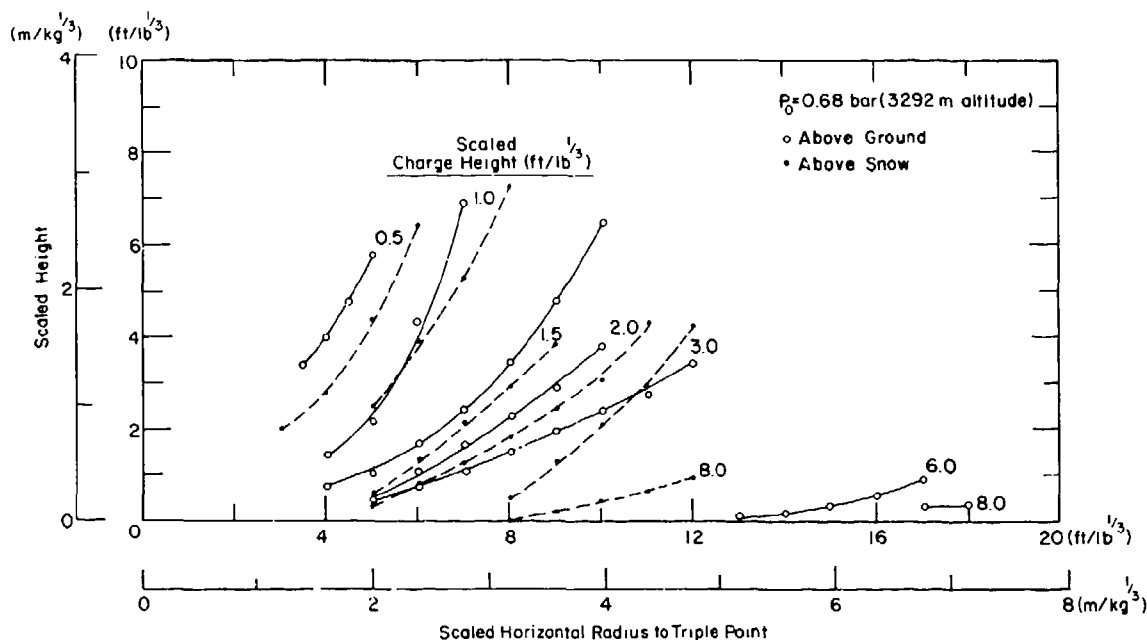
53

Figure 52. Height of triple point (Mach stem) as a function of radius and charge height for explosions over seasonal snow cover and over bare ground at high altitude. From Wisotski and Snyer (1966).

The path of the triple point over seasonal snow and over bare ground is shown in Figures 50 and 52. In general, the Mach stem is higher over bare ground than over snow at the same radius.

Wisotski and Snyer defined a reflection coefficient K as the ratio of charge weights which will produce equal overpressures at a given radial distance when: (a) the charge is fired in free air, and (b) the charge is fired close to the Mach reflection surface. Designating these charge weights as W_{FA} and W_{MR},

$$K = W_{FA}/W_{MR} \qquad (35)$$

If W_{MR} is taken as unit weight, K can be expressed in terms of scaled radii to a given contour of peak overpressure:

$$K = \left(\overline{r}_{MR} / \overline{r}_{FA} \right)^3 \qquad (36)$$

where $\overline{r}_{FA}$ is scaled radius in free air to peak incident overpressure level p_m, and $\overline{r}_{MR}$ is scaled radius to peak reflected pressure p_m in the Mach region. Values of K for bare ground, snow and concrete are plotted against scaled charge height in Figure 53.

54
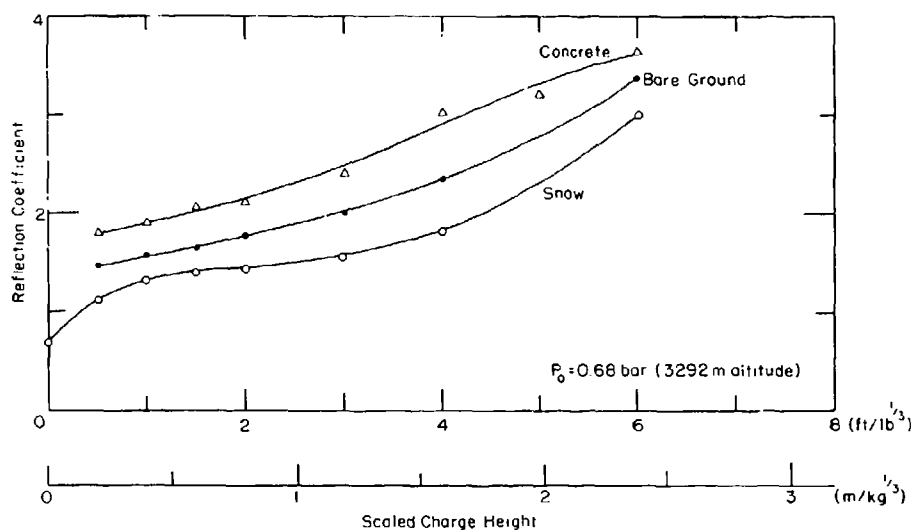
Figure 53. Reflection coefficient (see text) as a function
of charge height for snow, bare ground and concrete at high
altitude. From Wisotski and Snyer (1966).
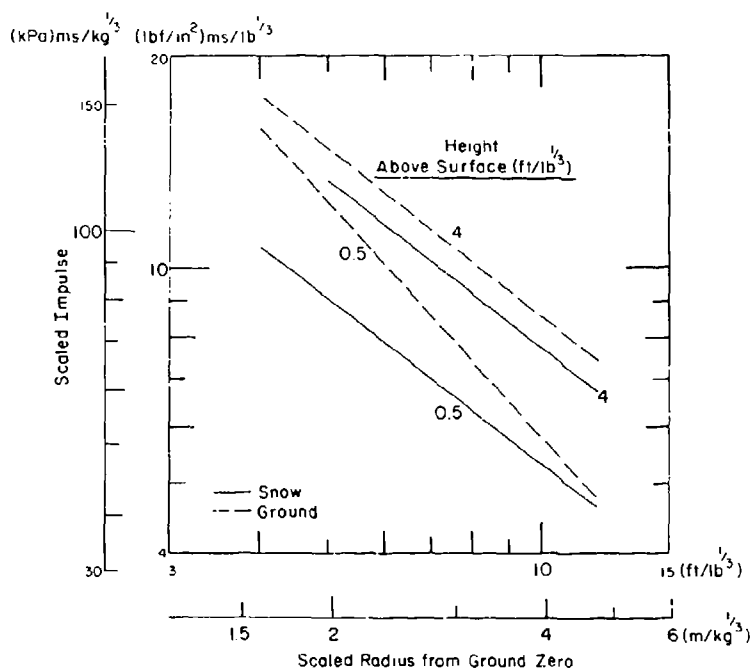
Figure 54. Positive impulse as a function
of radius and charge height for explosions
over seasonal snow cover and over bare
ground at high altitude. Summary of re-
sults by Wisotski and Snyer (1966).

55

Figure 54 (cont'd). Positive impulse as a function of radius and charge height for explosions over seasonal snow cover and over bare ground at high altitude. Summary of results by Wisotski and Snyer (1966).
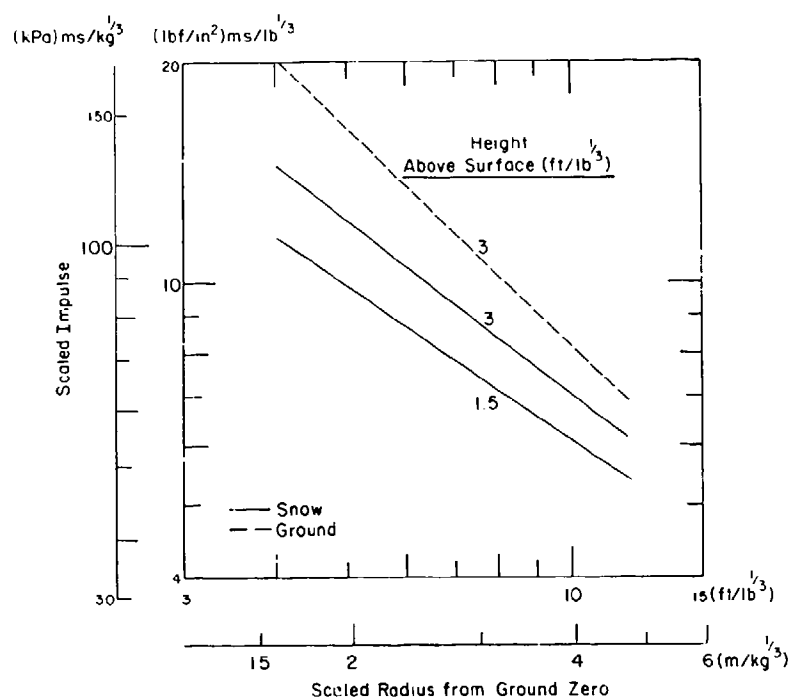
Figure 54 (cont'd).

Impulse measurements over seasonal snow and over bare ground gave fairly scattered data; trend lines are shown in Figure 54. In general, the impulse over bare ground is higher than the impulse over snow.
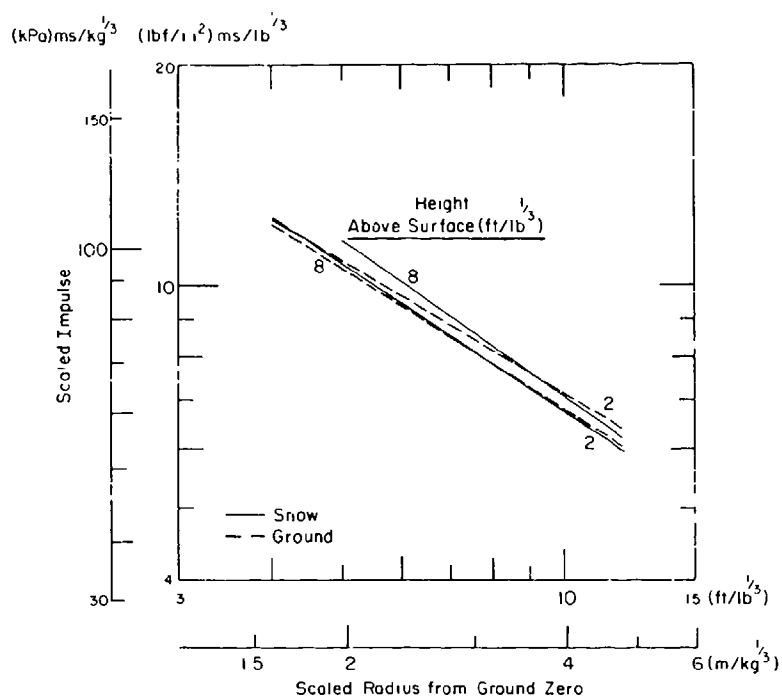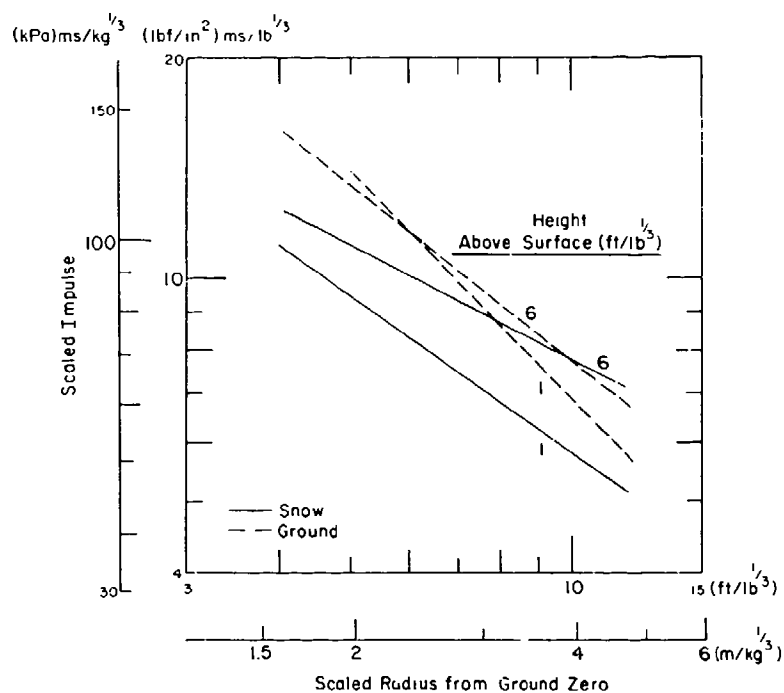
Shock reflection from a surface of land-based ice should not be significantly different from rigid-surface reflection. However, reflection from a floating ice cover could involve energy dissipation and reduction of amplitude in the reflected wave. At this time, no test data are available.

Shock Velocity Over Snow

Measurements of shock velocity were made on the Greenland ice cap (Fig. 55). They agree fairly well with the theoretical shock velocity, as calculated from eq 20. The discrepancies can probably be attributed to calibration errors in the pressure transducers, and perhaps to other problems in the measuring equipment (one set of data shows shock velocity dropping below the expected acoustic velocity).

57

Figure 55. Shock velocity as a function of peak over-
pressure for explosions over deep snow at high alti-
tude. After Smith (1962).

Variation of Shock Pressure with Charge Height Over Snow

At ground zero, the point on the surface directly below an air burst,
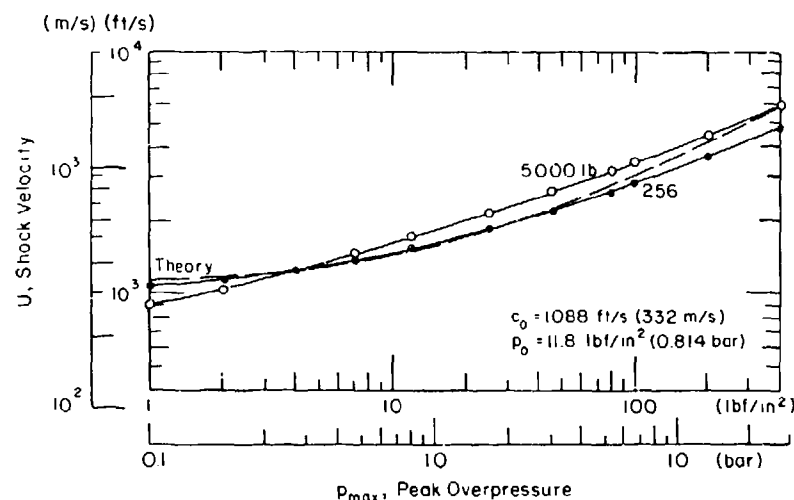peak overpressure decreases as charge height increases, in accordance with
the free-air attenuation relation. For a given charge height H, overpres-
sure decreases with horizontal radius from ground zero (R) in accordance
with the increase of slant range S from the charge, where $S = (H^2+R^2)^{1/2}$.
Figure 56 gives contours of peak overpressure for air blast over deep snow,
in the same form that is used for standard curves (see Fig. 12, 25). Fig-
ure 57 gives the data in another form, showing attenuation curves with
charge height as parameter.

The results of Wisotski and Snyer (1966) give attenuation curves mea-
sured over seasonal snow. Curves are given for a range of charge heights
(Fig. 46), and a free-air attenuation curve is included for comparison. At
any given radius from ground zero, the Mach region peak overpressure, p_m,
decreases as charge height increases, within the limited range of the data.
The results are shown in different form in Figure 51, which does not dis-
play the characteristic "bulges" seen in Figures 12 and 56 for somewhat
broader fields of coverage. For any finite charge height, p_m is higher
than the free-air value after Mach reflection from snow. However, for zero
charge height, with the charge lying in the snow, p_m is smaller than the
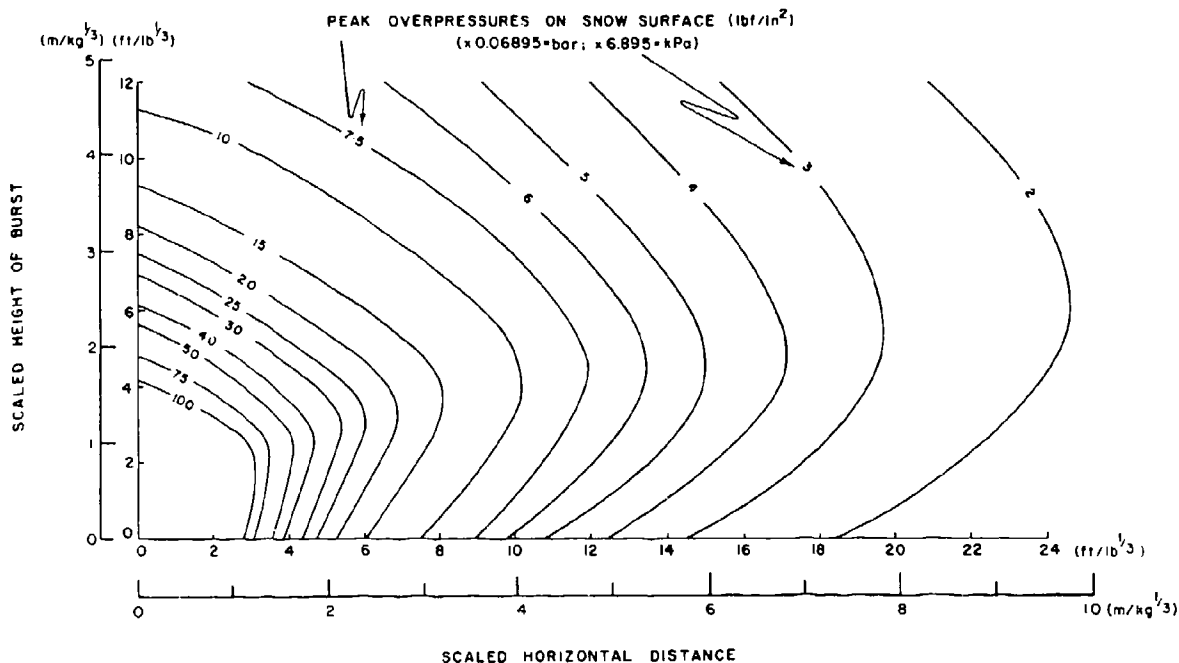free-air value.

58

Figure 56. Variation of peak overpressure with radius and charge height for explosions over deep snow at high altitude. From Ingram (1962).
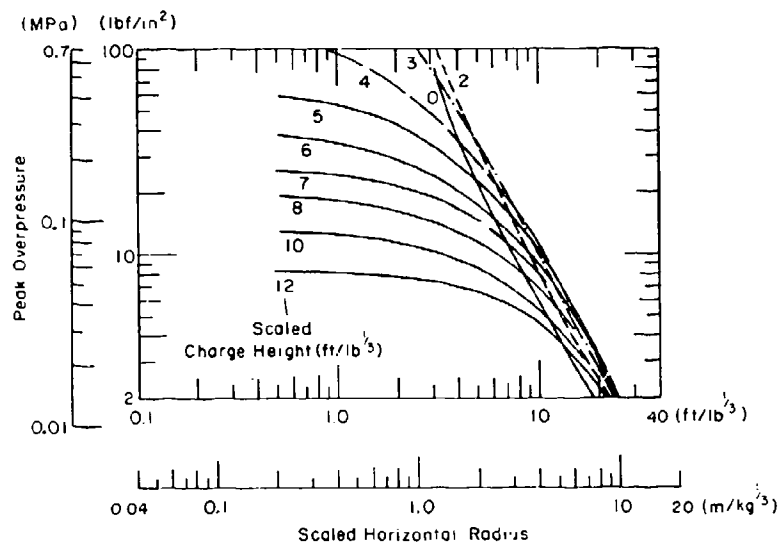

Figure 57. Peak overpressure as a function of radius and charge height for explosions over deep snow at high altitude. After Ingram (1962).

59

Release of Avalanches by Air Blast

Snow lying on a slope can slip and form an avalanche when the down-slope shear stress exceeds the shear strength at any level in the snow pack. Under natural circumstances, such instability develops when stress increases faster than strength because of rapid accumulation, or alternatively when snow strength deteriorates under constant stress. If a snow slope is highly stable (gentle slope, well-settled dry snow) it is unlikely to be disturbed by air blast. However, if the snow is only marginally stable (slope angle 30°-60°, stress/strength ratio approaching unity), then air blast could trigger an avalanche. The question is, how much overpressure is required, and over how wide an area must it be distributed?

Avalanche folklore includes instances of avalanche release by the sound of church bells, alpenhorns or bellowing voices, but it is hard to believe that such weak elastic waves have much effect. At the other extreme, marginally stable snow is very likely to be released by detonation of a concentrated charge bigger than 1 kg when the scaled charge height is about 4 $ft/lb^{1/3}$ (1.6 $m/kg^{1/3}$). The overpressure produced by such a charge can be seen by referring to Figures 12, 46, and 56; assuming a charge weight greater than 1 kg (2 lb), overpressures greater than 10 lbf/in.^{2} (70 kPa) are likely to be applied over a radius significantly greater than the thickness of the snowpack. However, this does not establish a lower limit for air blast release.

Sonic boom studies showed that avalanches can be triggered by wide-spread peak pressure of 2 lbf/ft^2 (0.014 lbf/in.^{2}, or 0.1 Pa). This is the pressure level at which sonic booms begin to have the ability to crack plaster and glass in surface structures. It is equivalent to the addition of 4 to 5 in. (100-130 mm) of low density snow (0.1 Mg/m^3) on slopes of typical angle for avalanche release zones. In air blast terms, it is the pressure that might be felt at a radius of 40 $m/kg^{1/3}$ (100 $ft/lb^{1/3}$) when a charge is fired just above the surface (say 0-5 $ft/lb^{1/3}$, or 0-2 $m/kg^{1/3}$).

For practical purposes, it has been suggested (Mellor 1973) that the target zone should be subjected to overpressures of at least 0.5 lbf/in.^{2} (3.5 Pa), perhaps by firing at a height of 5 $ft/lb^{1/3}$ (2 $m/kg^{1/3}$). For a charge of minimum size (1 lb, or 0.5 kg) this gives an effective target zone of diameter 100 ft, or 30 m.

References

Baker, W.E. (1973) Explosions in Air. University of Texas Press, 268 pp.

Brode, H.L. (1964) A review of nuclear explosion phenomena pertinent to protective construction (U). Rand Corporation, Santa Monica, California, R-425-PR. (AD 601 139).

Defense Nuclear Agency (1972) Capabilities of nuclear weapons (U). DNA, Washington, D.C., Effects Manual DNA EM-1.

du Pont (1977) Blasters' Handbook. E.I. du Pont de Nemours & Co. (Inc.), Wilmington, Delaware, 494 pp.

Glasstone, S. (Ed.) (1962) The effects of nuclear weapons. DA Pamphlet 39-3, 730 pp.

Hallanger, L.W. (1976) Interim field guide to nearshore underwater explosive excavation. U.S. Navy Civil Engineering Laboratory, Port Hueneme, California, Technical Report R843, 121 pp.

Hughes, B.C. (1968) Nuclear construction engineering technology. USA Nuclear Cratering Group, Livermore, California, Technical Report 2, 174 pp.

Ingram, L.F. (1962) Air blast in an arctic environment. USA Waterways Experiment Station, Technical Report 2-597.

Ingram, L.F. and S.H. Halper (1960) Measurements of explosion-induced shock waves in ice and snow, Greenland, 1957 and 1958. USA Waterways Experiment Station, Miscellaneous Paper 2-399.

Joachim, C.E. (1964) Structures in an arctic environment, Reports, Airblast and subsurface shock of high explosive tests. USA Waterways Experiment Station, Technical Report 1-649.

Johnson, S.M. (1971) Explosive excavation technology. USA Nuclear Cratering Group, Livermore, California, Technical Report 21, 229 pp.

Jones, G.H.S. (1962) Some comments on cratering. Suffield Experimental Station, Defence Research Board of Canada, Suffield Special Publication 22.

Mellor, M. (1965) Explosions and snow. USA Cold Regions Research and Engineering Laboratory, Monograph III-A3a.

Mellor, M. (1968) Avalanches. USA Cold Regions Research and Engineering Laboratory, Monograph III-A3d.

Mellor, M. (1973) Controlled release of avalanches by explosives. Symposium on Advances in Avalanche Technology, Reno, 1972, Technical Report RM-3, USDA Forest Service, p. 37-49.

61

Mellor, M. and N. Smith (1967) Airblast attenuation at low overpressures. USA Cold Regions Research and Engineering Laboratory, Technical Note (unpublished).

Siskind, D.E., V.J. Stachura, M.S. Stagg and J.W. Kopp (1980) Structure response and damage produced by airblast from surface mining. Bureau of Mines Report of Investigations RI 8485, 111 pp.

Smith, N. (1962) Air pressures and shock wave velocities from high explosive surface contact explosions over arctic snow surface. USA Cold Regions Research and Engineering Laboratory, Technical Note (unpublished).

Swisdak, M.M. (1975) Explosion effects in air. Naval Surface Weapons Center, Technical Report 75-116, 139 pp.

Swisdak, M.M. (1978) Explosion effects and properties: Part II – Explosion effects in water. Naval Surface Weapons Center, Technical Report 78-116, 109 pp.

Taylor, G. (1950) The formation of a blast wave by a very intense explosion. Proceedings of the Royal Society, 201(A): 159-186.

U.S. Army (1984) Designing facilities to resist nuclear weapon effects. Technical Manual 5-858-2.

Wisotski, J. and W.H. Snyer (1966) A study of the effects of snow cover on high explosive blast parameters. Denver Research Institute, Denver University, Report DU-DRI-2303, 97 pp.